Celestial Mechanics and Dynamical Astronomy (2023) 135:52
https://doi.org/10.1007/s10569-023-10164-1

ORIGINAL ARTICLE

Analyzing the structure of periodic orbit families that exist around asteroid (101955) Bennu

Gavin M. Brown[1] · Daniel J. Scheeres[1]

Received: 26 May 2023 / Revised: 21 August 2023 / Accepted: 18 September 2023

Abstract
Periodic orbit families that exist around the asteroid (101955) Bennu were computed and analyzed to gain insight into the dynamical environment about the asteroid. A constant-density polyhedron model was used to generate the families. The planar direct and retrograde families, and families emanating from equilibria, were computed. Ten distinct families were identified in this set, and many of the orbit structures were similar (e.g., the vertical families emanating from the equilibria behaved in similar ways), and several of these structures were connected to each other. We identified 12 distinct families emanating from bifurcation points in the initial families. These 12 families could be classified into four types. Even though the model of Bennu had no exact symmetry, many nearly symmetric structures were identified. There were also many similarities to structures identified using simplified models like the homogeneous rotating gravitating triaxial ellipsoid. The behavior of the identified families also provided insight into the evolution of the dynamical environment around the asteroid. We expect the qualitative behavior of the families we identified to be similar to the families that would exist around other asteroids that are nearly spherical.

Keywords Dynamics · Orbits · Asteroids · Bifurcations · Bennu

1 Introduction

Understanding the behavior and characteristics of the dynamical environment about celestial bodies is essential to the field of celestial mechanics. Analyzing the structure of orbit families that exist around these bodies is one component to understanding the dynamical environment. In recent years, there has been an increased scientific interest in developing missions to send spacecraft to study these bodies, particularly asteroids. One example of such a mission is the OSIRIS-REx mission. The spacecraft arrived at the asteroid (101955) Bennu in late

✉ Gavin M. Brown
gavin.m.brown@colorado.edu

Daniel J. Scheeres
scheeres@colorado.edu

1 Department of Aerospace Engineering Sciences, University of Colorado Boulder, 3775 Discovery Drive, Boulder, CO 80303, USA

2018 (Lauretta et al. 2019; McMahon et al. 2020). While this study has some implications for mission design, that is not our primary focus. In this paper, we undertake a mathematical exploration of the complex periodic orbit bifurcation structure about a “real” asteroid that has asymmetry. This paper seeks to address how asymmetries can modify the periodic orbit family structure. The characteristics of an asteroid, such as its size, density, and spin rate, can affect the dynamical environment, including the structure of orbit families. The density, strength, and other characteristics and properties of asteroids, including rubble-pile asteroids such as Bennu, have been studied previously (Scheeres et al. 2015; Benner et al. 2015).

Equilibrium points (EPs) that exist in the vicinity of the asteroid are important for analyzing the dynamical environment. These equilibria are relevant to this work as orbit families are known to emanate from these points. The equilibria, and their evolution, have been studied around a number of asteroids (Jiang and Baoyin 2018), including Bennu (Scheeres et al. 2016; Brown and Scheeres 2023b). Determining the locations and properties of these equilibria can be accomplished in a number of ways (Tardivel 2014; Brown and Scheeres 2023a), and the method outlined in Tardivel (2014) has the added benefit of yielding the ridge line as well.

1.1 Previous research

Orbit families have been previously mapped out in simpler models, such as the Circular Restricted 3-Body Problem (CR3BP) and the homogeneous rotating gravitating triaxial ellipsoid (HRGTE or TAEM). As the structure of the linearized systems for each of the models is similar (Tardivel 2014), these orbit families will serve as a reference point for analyzing the families identified in this work. A look at the qualitative behavior and structure of generating families in the CR3BP was presented in Hénon (1997). A road map in the form of a bifurcation diagram of families existing in the CR3BP has also been developed (Doedel et al. 2007). Similar bifurcation diagrams for orbit families about the equilibria of the system have been developed for the TAEM and the massive rotating straight segment (MRSS) (Romanov and Doedel 2012, 2014). A far more detailed bifurcation diagram was presented for several orbit families in the CR3BP to model motion near Europa (Bury 2021). The stability of orbits in these types of systems can be determined by using the stability parameters and Broucke stability diagram (Broucke 1969). The effects of non-spherical terms on the structure and stability of orbit families initially existing in the 2-body problem have also been studied (Hou et al. 2018).

The particular behavior of the periodic orbits about an asteroid are closely tied to the form of the potential. Modeling the gravity field with a spherical harmonic expansion was one of the first approaches used to analyze the dynamical environment about asteroids (MacMillan 1958). There are many ways to represent the gravity field around asteroids, but we will use a gravity model based on the representation of the asteroid as a constant-density polyhedron. The exterior gravitation of this model was presented in Werner and Scheeres (1996). The accuracy of this model is primarily limited by the accuracy in the shape determination of the body and its discretization (Werner and Scheeres 1996). The error associated with using this model with the assumption that the density of the asteroid is constant was measured to be a few percent when considering measurements from the OSIRIS-REx mission to Bennu (Scheeres et al. 2020).

The direct and retrograde orbits around (433) Eros have been studied using a spherical harmonic expansion to model the gravity field (Scheeres et al. 2000). A few resonant families using this type of model around Eros have also been studied (Lara and Scheeres 2002). A second degree and order gravity field has also been used to study orbits around

(4769) Castalia (Hu and Scheeres 2008). Chappaz (2011) used both a model based on spherical harmonics and a model based on a constant-density polyhedron to compute the direct and retrograde families about Eros, Castalia, and Mars' moon Phobos. Certain resonant families identified in bifurcations on the direct and retrograde families were also studied in that work (Chappaz 2011). The stable and unstable regions for retrograde orbits about (216) Kleopatra, (243) Ida, Eros, and three other asteroids, have been computed modeling each asteroid as a polyhedron (Lan et al. 2017). While gravity models based on spherical harmonics and polyhedrons are often used when studying asteroids, other types of models can be used. For example, Lan et al. (2017) also computed the unstable regions for retrograde orbits using a double-particle-linkage model for Kleopatra and (951) Gaspra, and a triple-particle-linkage model for Ida and Eros. Periodic orbits around a rotating homogeneous body with a dumbbell shape and transfers between some of these orbits, and have also been studied (Li et al. 2017).

Beyond the orbits related to the direct and retrograde families, orbit families around the equilibria in these types of systems have also been studied. Periodic orbits and trajectories on the stable and unstable manifolds associated with the equilibria around Castalia have been computed and analyzed (Scheeres et al. 1996). Mathematical descriptions of the orbits and manifolds about equilibria around asteroids have been developed and applied to compute both periodic and quasi-periodic orbits around Kleopatra, (1620) Geographos, Castalia, and (6489) Golevka using a polyhedron gravity model (Jiang et al. 2014). Initial orbits on the families can be obtained through appropriate analysis of the linearized motion about equilibria of the system. However, while some form of numerical continuation is normally used when computing orbit families in these systems, there are a multitude of approaches to obtain an initial set of orbit members. For example, a "hierarchical grid searching method" to compute periodic orbits was developed and applied to compute orbits about a polyhedron model of Kleopatra (Yu and Baoyin 2012a). Using this method 29 families were identified, including six which emanated from equilibria (Yu and Baoyin 2012a, b). The same method has also been applied to (22) Kalliope and Ida (Jiang and Li 2019; Yu et al. 2015).

Considering the progression and evolution of orbit families in these systems is also of interest. How the characteristics of orbits change along one family will be referred to as the "progression" of that family. How the characteristics of the orbits on a family, and the structure of the family as a whole, change as parameters describing the asteroid's gravity field vary will be referred to as the "evolution" of that family. The progression of orbits in families near the surface of Kalliope, Kleopatra, and Eros have been studied previously using constant-density polyhedron gravity models (Kang et al. 2020). Variations in the shape of the asteroid have been considered for Eros using shape continuation when computing orbits (Karydis et al. 2021). How families fit together is also important to consider when analyzing periodic orbits in these systems. Bifurcation points along an orbit family are important to track as they can be used to identify additional orbit families in some instances (Broucke 1969; Howard and MacKay 1987; Campbell 1999). With that in mind, bifurcation diagrams can be used to depict connections between different orbit families. Bifurcation points on specific orbit families in the vicinity of the comet 1P/Halley and the asteroid Kleopatra have been computed (Jiang and Baoyin 2016). In addition to identifying bifurcation points on orbit families around 1P/Halley, Kleopatra, and Golevka, Jiang et al. (2015b) also presented 34 topological classifications for the types of periodic orbits identified around irregular-shaped bodies. These classifications, and possible bifurcation paths on the periodic orbits, were studied further for polyhedron models representing Kleopatra and Bennu (Jiang et al. 2015a), as well as Eros (Ni et al. 2016). Two high-level bifurcation diagrams for periodic orbit families emanating from the equilibria of an irregular-shaped body have been constructed previously (Jiang and Baoyin

2019). However, the diagrams presented in Jiang and Baoyin (2019) are only applicable in cases where the asteroid of interest has only four external equilibria, like Kleopatra and Eros.

While only the rotation and gravitational attraction of the asteroid will be considered in this work, it is important to note that in order to use these orbits in higher fidelity models, additional effects and perturbations will need to be considered. The effect of solar perturbations on several of the families identified in Yu and Baoyin (2012a), and a few families around Eros, have been studied (Ni et al. 2014). In addition to considering the effect of solar perturbations, the effect of different gravity models have been analyzed on orbits around (341843) 2008 EV5 (Llanos et al. 2014). The effect of solar radiation pressure (SRP) and thermal radiation pressure (TRP) on several periodic orbits in the vicinity of Bennu have also been studied (Pedros-Faura and McMahon 2022).

1.2 Current work

As this work focuses specifically on Bennu, it is important to highlight the previous research into orbits around this particular asteroid and the contributions of our current work. Beyond the orbits presented in Jiang et al. (2015a), the orbit members and bifurcation points on a vertical family about one of the equilibrium points and a 2:1 resonant family around Bennu have been computed previously (Liu et al. 2022). However, these computations were performed using a different shape model of the asteroid than the one used in this work. It is also important to note that portions of the orbit families presented in this work were first identified in Scheeres et al. (2022). However, the families presented in that paper were incomplete and slight modifications have been made to the shape model of Bennu that was used in that work (Scheeres et al. 2022). While a number of orbit families around Bennu have been identified previously, this work presents the most comprehensive collection of orbit families around this asteroid to date. We continue the families beyond the point where a member intersects the surface of the asteroid, which provides a more complete picture of the orbit structures that exist. Furthermore, this work uses estimates of Bennu's characteristics and shape based on measurements from the OISRIS-REx mission. The specific shape model we used is the image-based stereophotoclinometry (SPC) v42 model (Barnouin et al. 2019), which can be found in the JHUAPL Small Body Mapping Tool (SBMT).

In Sect. 2, we will present the dynamical model and discuss the stability and characteristics of periodic orbits in these types of systems. In Sect. 3, we will outline the method we use to compute and analyze different orbit families. We will then present the orbit families we identified and discuss their properties in Sect. 4. In this section, we will also discuss the similarities in the families we identified and the orbit families that exist in simplified dynamical models. Finally, we will comment on whether we expect these results to be similar to orbit families that exist around other asteroids.

2 Problem statement

2.1 Coordinate frames and scaling

To begin we assume that the asteroid is rotating at a constant angular velocity $\boldsymbol{\omega}$ with a constant magnitude ω and direction $\hat{z}$. Let $\mathcal{B} : \left\{\hat{x}, \hat{y}, \hat{z}\right\}$ be a rotating frame with an origin at the center of the asteroid and angular velocity $\boldsymbol{\omega} = \omega\hat{z}$. Note that the mass distribution remains constant in the $\mathcal{B}$-frame (Tardivel 2014). The normalized units defined in Eq. 1 are used for most computations in this work.

$$1 \text{ DU} = \left(\frac{3A_V}{4\pi}\right)^{1/3} \tag{1a}$$

$$1 \text{ TU} = \frac{1}{\omega} \tag{1b}$$

Distance is scaled by the radius of the sphere that has the same volume (A_V) as the asteroid. Time is scaled so the rotation period of the asteroid is 2π TU, which results in an angular velocity of $\omega = 1$ rad TU^{-1}. The values of A_V and ω used in Eq. 1 should be dimensional quantities.

2.2 Defining the model

Bennu is represented as a uniformly rotating constant-density polyhedron in this work. Please refer to Tardivel (2014), MacMillan (1958), and Werner and Scheeres (1996) for a more rigorous discussion of the potential and broad dynamical features associated with this type of model. The shape model is based off of data collected during the OSIRIS-REx mission (McMahon et al. 2020; Barnouin et al. 2019). We used a model with 12,228 faces to maintain a highly accurate representation of the asteroid, while also ensuring the computational cost associated with the model was not prohibitively excessive. We also used a model with 3,072 faces to test the sensitivity of the orbit structures to the discretization of the model. We assume Bennu has a constant uniform density $\sigma = 1190$ kg m^{-3} and a rotation period of $T_{\text{rot}} = 4.296057$ hr (Barnouin et al. 2019; Hergenrother et al. 2019; Lauretta et al. 2019). Note that the spin rate ω corresponding to T_{rot} can be determined by using the following relationship: $\omega = 2\pi/T_{\text{rot}}$. The gravitational force potential U for a constant-density polyhedron, and the partial derivatives of U with respect to the position in the body-fixed frame $\boldsymbol{r}$, are provided in Eq. 2 (Werner and Scheeres 1996). Besides U, the other expressions in Eq. 2 are the gravitational attraction (∇U), gravity gradient matrix ($\nabla\nabla U$), and Laplacian ($\nabla^2 U$ or ΔU).

$$U = \frac{1}{2} G\sigma \sum_{\text{e}=1}^{n_\text{e}} \boldsymbol{r}_\text{e} \cdot \boldsymbol{E}_\text{e} \cdot \boldsymbol{r}_\text{e} \cdot L_\text{e} - \frac{1}{2} G\sigma \sum_{\text{f}=1}^{n_\text{f}} \boldsymbol{r}_\text{f} \cdot \boldsymbol{F}_\text{f} \cdot \boldsymbol{r}_\text{f} \cdot \omega_\text{f} \tag{2a}$$

$$\nabla U = -G\sigma \sum_{\text{e}=1}^{n_\text{e}} \boldsymbol{E}_\text{e} \cdot \boldsymbol{r}_\text{e} \cdot L_\text{e} + G\sigma \sum_{\text{f}=1}^{n_\text{f}} \boldsymbol{F}_\text{f} \cdot \boldsymbol{r}_\text{f} \cdot \omega_\text{f} \tag{2b}$$

$$\nabla\nabla U = G\sigma \sum_{\text{e}=1}^{n_\text{e}} \boldsymbol{E}_\text{e} \cdot L_\text{e} - G\sigma \sum_{\text{f}=1}^{n_\text{f}} \boldsymbol{F}_\text{f} \cdot \omega_\text{f} \tag{2c}$$

$$\Delta U = -G\sigma \sum_{\text{f}=1}^{n_\text{f}} \omega_\text{f} = \text{tr}\left(\nabla\nabla U\right) = \begin{cases} 0 & \text{outside the body} \\ -4\pi G\sigma & \text{inside the body} \end{cases} \tag{2d}$$

In Eq. 2, G is the gravitational constant and σ is the density of the asteroid. n_e is the number of edges and n_f is the number of faces of the polyhedron. Additional expressions needed to evaluate Eq. 2 are provided in Eq. 3 (Werner and Scheeres 1996).

$$\boldsymbol{E}_\text{e} = \hat{\boldsymbol{n}}_{f_{\text{e},1}} \left(\hat{\boldsymbol{n}}_\text{e}^{f_{\text{e},1}}\right)^T + \hat{\boldsymbol{n}}_{f_{\text{e},2}} \left(\hat{\boldsymbol{n}}_\text{e}^{f_{\text{e},2}}\right)^T \tag{3a}$$

$$L_\text{e} = \ln \frac{r_{i_\text{e}} + r_{j_\text{e}} + l_\text{e}}{r_{i_\text{e}} + r_{j_\text{e}} - l_\text{e}} \tag{3b}$$

$$\boldsymbol{F}_{\mathrm{f}} = \hat{\boldsymbol{n}}_{\mathrm{f}}\hat{\boldsymbol{n}}_{\mathrm{f}}^{T} \tag{3c}$$

$$\omega_{\mathrm{f}} = 2\arctan\frac{\boldsymbol{r}_{i_{\mathrm{f}}}\cdot\boldsymbol{r}_{j_{\mathrm{f}}}\times\boldsymbol{r}_{k_{\mathrm{f}}}}{r_{i_{\mathrm{f}}}r_{j_{\mathrm{f}}}r_{k_{\mathrm{f}}} + r_{i_{\mathrm{f}}}\left(\boldsymbol{r}_{j_{\mathrm{f}}}\cdot\boldsymbol{r}_{k_{\mathrm{f}}}\right) + r_{j_{\mathrm{f}}}\left(\boldsymbol{r}_{k_{\mathrm{f}}}\cdot\boldsymbol{r}_{i_{\mathrm{f}}}\right) + r_{k_{\mathrm{f}}}\left(\boldsymbol{r}_{i_{\mathrm{f}}}\cdot\boldsymbol{r}_{j_{\mathrm{f}}}\right)} \tag{3d}$$

$\boldsymbol{P}_i$ represents the position of the i^{th} vertex. Assuming the polyhedron consists of triangular faces, face f is the triangle whose vertices are located at $\boldsymbol{P}_{i_{\mathrm{f}}}$, $\boldsymbol{P}_{j_{\mathrm{f}}}$, $\boldsymbol{P}_{k_{\mathrm{f}}}$. Each face f also has an outward-pointing face normal vector $\hat{\boldsymbol{n}}_{\mathrm{f}}$ and face dyad $\boldsymbol{F}_{\mathrm{f}}$. Edge e connects two vertices $\boldsymbol{P}_{i_{\mathrm{e}}}$, $\boldsymbol{P}_{j_{\mathrm{e}}}$ and separates two of the faces $f_{\mathrm{e},1}$, $f_{\mathrm{e},2}$. Each edge e has a constant length l_{e} and has an edge dyad $\boldsymbol{E}_{\mathrm{e}}$. $\hat{\boldsymbol{n}}_{\mathrm{e}}^{\mathrm{f}}$ is the unit vector perpendicular to both $\hat{\boldsymbol{n}}_{\mathrm{f}}$ and $\hat{\boldsymbol{l}}_{\mathrm{e}}$. The expressions for $\boldsymbol{E}_{\mathrm{e}}$ and $\boldsymbol{F}_{\mathrm{f}}$ are presented in matrix notation. For some point in the body-fixed frame $\boldsymbol{r}$, $\boldsymbol{r}_i$ represents the position of the vertex located $\boldsymbol{P}_i$ relative to $\boldsymbol{r}$. $\boldsymbol{r}_i$ has a magnitude of r_i.

To consider motion in the rotating frame, the rotational effects must also be considered. The amended potential (V), defined in Eq. 4, includes gravitational and rotational effects (Scheeres et al. 2016; Tardivel 2014). The force $\boldsymbol{F}$ resulting from V is related to the gradient of V by $\boldsymbol{F} = -\nabla V$ (Tardivel 2014). The derivatives of the potential that will be needed to evaluate the equations of motion and conduct stability analysis are also provided in Eq. 4.

$$V = -U - \frac{1}{2}\left\|\boldsymbol{\omega}\times\boldsymbol{r}\right\|^2 \tag{4a}$$

$$\nabla V = -\nabla U + \boldsymbol{\omega}\times(\boldsymbol{\omega}\times\boldsymbol{r}) = \begin{bmatrix} V_x \\ V_y \\ V_z \end{bmatrix} \tag{4b}$$

$$\nabla\nabla V = -\nabla\nabla U + \left[\tilde{\boldsymbol{\omega}}\right]\left[\tilde{\boldsymbol{\omega}}\right] = \begin{bmatrix} V_{xx} & V_{xy} & V_{xz} \\ V_{yx} & V_{yy} & V_{yz} \\ V_{zx} & V_{zy} & V_{zz} \end{bmatrix} \quad \text{where} \quad \left[\tilde{s}\right] = \begin{bmatrix} 0 & -s_3 & s_2 \\ s_3 & 0 & -s_1 \\ -s_2 & s_1 & 0 \end{bmatrix} \tag{4c}$$

$$\Delta V = \operatorname{tr}(\nabla\nabla V) = -\Delta U + \operatorname{diag}\left(\left[\tilde{\boldsymbol{\omega}}\right]\left[\tilde{\boldsymbol{\omega}}\right]\right) = -\Delta U - 2\omega^2 \tag{4d}$$

Note that subscripts on the potential represent the partial derivative(s) with respect to the variable(s) in the subscript. A numerical subscript on a vector indicates the component of a vector.

2.3 Equations of motion

The state vector of some particle is represented by $\boldsymbol{X} = \left[\boldsymbol{r}^T\ \boldsymbol{v}^T\right]^T$ where $\boldsymbol{r}$ and $\boldsymbol{v}$ are the position and velocity in the $\mathcal{B}$-frame, respectively. The state transition matrix is represented by $[\Phi(t, t_0)] = \frac{\partial\boldsymbol{X}}{\partial\boldsymbol{X}_0}$ and the Jacobian matrix is represented by $[A] = \frac{\partial\dot{\boldsymbol{X}}}{\partial\boldsymbol{X}}$. Let $\boldsymbol{X}(t_0) = \boldsymbol{X}_0$ and note $[\Phi(t_0, t_0)] = \left[I_{6\times6}\right]$. Equation 5 presents the equations of motion for a particle whose mass is negligible compared to the mass of the asteroid.

$$\dot{\boldsymbol{X}} = \boldsymbol{f}(\boldsymbol{X}) = \begin{bmatrix} \boldsymbol{v} \\ -2\boldsymbol{\omega}\times\boldsymbol{v} - \nabla V \end{bmatrix} \tag{5a}$$

$$\left[\dot{\Phi}(t, t_0)\right] = [A(t)]\left[\Phi(t, t_0)\right] \tag{5b}$$

$$[A] = \begin{bmatrix} \left[0_{3\times3}\right] & \left[I_{3\times3}\right] \\ -\nabla\nabla V & -2\left[\tilde{\boldsymbol{\omega}}\right] \end{bmatrix} \tag{5c}$$

Note $[A]$ represents the linearized dynamics about some point and does not explicitly depend on time because the system is time-invariant. However, $[A]$ will evolve in time when it is evaluated along some nominal trajectory if the state on the nominal trajectory changes in time. For a state perturbation ($\delta \boldsymbol{X}$) relative to a reference state on the nominal trajectory, the time rate of change of the perturbation is $\delta \dot{\boldsymbol{X}} = [A]\, \delta \boldsymbol{X}$. If the initial perturbation at t_0 is $\delta \boldsymbol{X}_0$, then the perturbation at t is $\delta \boldsymbol{X} = [\Phi(t, t_0)]\, \delta \boldsymbol{X}_0$ (Scheeres 2012).

It is important to note that there is a conserved quantity in the rotating frame for this system referred to as the Jacobi energy (C) (Scheeres et al. 2016). The Jacobi energy is the same as the Hamiltonian for this time-invariant system, and is also referred to as the Jacobi constant or the Jacobi integral (Scheeres 2012). An expression for this quantity is presented in Eq. 6.

$$C = H(\boldsymbol{X}) = \frac{1}{2} v^2 + V \tag{6}$$

2.4 Stability of periodic orbits

For a state on a periodic orbit $\boldsymbol{X}_0$ at time $t_0 = 0$, the state transition matrix after one period $[\Phi_M] = [\Phi(T, 0)]$ is referred to as the monodromy matrix, where T is the period. If $\boldsymbol{X}(T) = \boldsymbol{X}_\mathrm{f}$, then for a periodic orbit $\boldsymbol{X}_\mathrm{f} = \boldsymbol{X}_0$. The stability of a periodic orbit can be determined by analyzing the eigenvalues of its monodromy matrix. As the system is time-invariant, this matrix should always have at least two unity eigenvalues. As described in Scheeres (2012), these two unity eigenvalues can be eliminated by reducing the monodromy matrix to a linearized Poincaré map ($\left[\Phi_M^\mathrm{R}\right]$). This process effectively reduces the dimensionality of the problem from six to four, and the stability of the orbit can be determined by computing the two parameters A and B related to the Broucke stability diagram (Broucke 1969; Howard and MacKay 1987).

To perform this reuction, we must specify an appropriate reference state ($\boldsymbol{X}_0$), surface of section constraint ($S(\boldsymbol{r}_0) = 0$ where $\hat{\boldsymbol{s}}^T \boldsymbol{v}_0 \neq 0$), and fix the Jacobi energy of permissible deviated states ($H(\boldsymbol{X}_0 + \delta \boldsymbol{X}_0)$) to be the same as the Jacobi energy of the reference state (C_0). The reduced state is a 4×1 vector that will be represented by $\boldsymbol{Y}$, and every set of $\boldsymbol{Y}$, S, and C can be mapped to a unique $\boldsymbol{X}$. The full process and underlying assumptions are presented in Scheeres (2012), but we will provide a short summary of the relevant equations here. The form of these equations assumes the surface of section is related to the value of one position coordinate, the equation for the Jacobi constant is of the form shown in Eq. 6, and that integrating the initial state from the initial time t_0 to the time t_1 corresponds to another crossing of the surface of section (i.e., $S(\boldsymbol{X}_1) = 0$).

Regarding the surface of section constraint, let l_PS represent the position coordinate corresponding to a surface of section and v_PS represent the value. Let $\hat{\boldsymbol{s}}$ be a 3×1 vector whose elements are zero except for the l_PSth element which is one. For example, using this notation, $l_\mathrm{PS} = 2$ and $v_\mathrm{PS} = 0.5$ corresponds to a surface of section at $y = 0.5$ and $\hat{\boldsymbol{s}} = [0\ 1\ 0]^T$. The equation S can be used to define a surface of section of this form: $S(\boldsymbol{X}) = \hat{\boldsymbol{s}}^T \boldsymbol{r} - v_\mathrm{PS}$ which has a value of 0 when evaluated at points on the surface of section. Let $[D]$ be the 4×6 matrix that would be obtained by eliminating the $l_\mathrm{PS}^\mathrm{th}$ and $(l_\mathrm{PS} + 3)^\mathrm{th}$ rows of the 6×6 identity matrix.

$$\delta \boldsymbol{X}_0 = ([P_0] + [P_H]) \delta \boldsymbol{Y}_0 \tag{7a}$$

$$\left[\Phi_{1,0}^\mathrm{R}\right] = [P_0]^T\, [P_S]\, [\Phi(t_1, t_0)]\, ([P_0] + [P_H]) \tag{7b}$$

$$[P_0] = [D]^T \tag{7c}$$

$$[P_H] = -\frac{1}{\hat{\boldsymbol{s}}^T \boldsymbol{v}_0} \begin{bmatrix} 0_{3\times1} \\ \hat{\boldsymbol{s}} \end{bmatrix} \left([D] \left. \frac{\partial H}{\partial \boldsymbol{X}} \right|_{X_0} \right)^T \tag{7d}$$

$$[P_S] = \left[I_{6\times6} \right] - \frac{1}{\hat{\boldsymbol{s}}^T \boldsymbol{v}_1} \boldsymbol{f}(\boldsymbol{X}_1) \begin{bmatrix} \hat{\boldsymbol{s}} \\ 0_{3\times1} \end{bmatrix}^T \tag{7e}$$

We use $t_1 = T$ such that $[\Phi(t_1, t_0)] = [\Phi_M]$ and $\left[\Phi^{\mathrm{R}}_{1,0}\right] = \left[\Phi^{\mathrm{R}}_M\right]$ in Eq. 7b. The eigenvectors of $\left[\Phi^{\mathrm{R}}_M\right]$ will be 4×1, but can be represented in the full state space by using Eq. 7a. The stability parameters A and B can be computed using Eq. 8 where "$\mathrm{Tr}\,([L])$" indicates the trace of the matrix $[L]$ (Broucke 1969; Howard and MacKay 1987).

$$A = \mathrm{Tr}\left(\left[\Phi^{\mathrm{R}}_M\right]\right) \tag{8a}$$

$$B = \frac{1}{2}\left(A^2 - \mathrm{Tr}\left(\left[\Phi^{\mathrm{R}}_M\right]^2\right)\right) \tag{8b}$$

The periodic orbit is stable if $B \geq 2A - 2$, $B \geq -2A - 2$, $B \leq \frac{1}{4}A^2 + 2$, and $B \leq 6$ (Broucke 1969). These parameters can also be used to identify bifurcation points, which will be discussed in more detail in Sect. 3.2.2.

2.5 Convention for describing periodic orbits

In this paper "orbit" will refer to a periodic orbit and "family" will refer to a periodic orbit family. The term "structure" will refer to the general behavior of the orbit families such as their characteristics, their properties, etc. It can also refer to how orbit families intersect with each other. "Symmetric" means that the object Γ is invariant under some given symmetry defined by the transformation Σ (Hénon 1997). An orbit or a family will be called "nearly symmetric" if it is close to being symmetric, but not exactly. "Γ' is symmetrical of Γ" means the object Γ' is obtained from $\Sigma\Gamma$ (Hénon 1997). "Evolution" will refer to how the members of an orbit family (or structure) and their properties change as the spin rate (or other parameters of the asteroid) changes. "Progression" will refer to how the members of an orbit family (or structure) and their properties change as you continue between members. "Lyapunov" (with quotation marks) will be used when describing orbits that are similar to part of a $\boldsymbol{L}_i$ family in the TAEM (Romanov and Doedel 2012). "Vertical" (with quotation marks) will be used when describing orbits that are similar to part of a $\boldsymbol{V}_i$ family in the TAEM (Romanov and Doedel 2012), or to describe orbits with a significant out-of-plane amplitude.

3 Methodology

In this section, we will discuss the method we used to compute the periodic orbit families around Bennu. A pseudo-arclength continuation scheme was used when computing all of the families, so we will begin by outlining this continuation scheme and its termination conditions. An initial guess is needed to start the continuation scheme when computing a specific family, so we will then present how we obtain initial guesses for each of the orbit families presented in this work. These families include the planar direct and retrograde families, orbit families emanating from the equilibria, and orbit families emanating from bifurcations in those initial families.

3.1 Computing orbit families

We expect periodic orbits in this system to exist in one-parameter families. So, if we have identified one periodic orbit we expect to be able to identify a nearby periodic orbit that lies on the same family. We use a pseudo-arclength continuation scheme to compute the members of each orbit family. How to generate the first member of each family will be discussed later in Sect. 3.2. In this work, each orbit member is computed by correcting an initial guess for that member using a single shooting method with the free variables ($\boldsymbol{V}$), constraints ($\boldsymbol{G} = \boldsymbol{0}$ and $\boldsymbol{H} = \boldsymbol{0}$), and corrections Jacobian matrices ($[DG]$ and $[DH]$) provided in Eq. 9.

$$\boldsymbol{V} = \begin{bmatrix} \boldsymbol{X}_0 \\ T \end{bmatrix} \tag{9a}$$

$$\boldsymbol{G} = \begin{bmatrix} \boldsymbol{X}_\mathrm{f} - \boldsymbol{X}_0 \\ \boldsymbol{V}^T \hat{\boldsymbol{p}} - v_\mathrm{PS} \\ (\boldsymbol{V} - {}_{i-1}{}^{*}\boldsymbol{V})^T \, {}_{i-1}{}^{*}\hat{\boldsymbol{n}} - \Delta s \end{bmatrix} \tag{9b}$$

$$[DG] = \frac{\partial \boldsymbol{G}}{\partial \boldsymbol{V}} = \begin{bmatrix} [\Phi(T,0)] - \left[I_{6\times 6}\right] & \dot{\boldsymbol{X}}_\mathrm{f} \\ & \hat{\boldsymbol{p}}^T & \\ & {}_{i-1}{}^{*}\hat{\boldsymbol{n}}^T & \end{bmatrix} \tag{9c}$$

$$\boldsymbol{H} = \left[\boldsymbol{X}_\mathrm{f} - \boldsymbol{X}_0\right] \tag{9d}$$

$$[DH] = \frac{\partial \boldsymbol{H}}{\partial \boldsymbol{V}} = \left[[\Phi(T,0)] - \left[I_{6\times 6}\right] \; \dot{\boldsymbol{X}}_\mathrm{f}\right] \tag{9e}$$

$\boldsymbol{G}$ and $[DG]$ are used when correcting individual orbit members, while $\boldsymbol{H}$ and $[DH]$ are used when continuing from one orbit member to the next. Regarding notation, ${}_i{}^j\boldsymbol{V}$ represents the $\boldsymbol{V}$ (free variables vector) corresponding to the i^th orbit member after the j^th iteration of the correction scheme. A left superscript * represents the final $\boldsymbol{V}$ that satisfies the constraints, and a left superscript ^{0} represents the initial guess of $\boldsymbol{V}$ for that orbit member. $\boldsymbol{X}_k^l$ represents the l^th element of the 6×1 state vector at some time $t = t_k$. If there is no right superscript, then that indicates the entire vector is used. $k = 0$ corresponds to $t_0 = 0$, and ($k = \mathrm{f}$) corresponds to $t_\mathrm{f} = T$. Note that $\boldsymbol{X}_\mathrm{f}$ corresponds to the state obtained by integrating $\boldsymbol{X}_0$ from $t_0 = 0$ to $t_\mathrm{f} = T$ using Eq. 5. $\hat{\boldsymbol{p}}$ is a 7×1 vector whose elements are zero except $\hat{\boldsymbol{p}}^{l_\mathrm{PS}} = 1$. ${}^*\hat{\boldsymbol{n}}$ is a 7×1 vector that lies in the nullspace of ${}^*[DH]$. Δs is related to the desired step size between orbit members. The difference between the free variable vectors corresponding to the $(i-1)^\mathrm{th}$ and i^th members (${}_i{}^*\boldsymbol{V} - {}_{i-1}{}^*\boldsymbol{V}$) projected onto the expected direction of the family at the $(i-1)^\mathrm{th}$ member (${}_{i-1}{}^*\hat{\boldsymbol{n}}$) should be equal to Δs. When correcting a particular member, Eq. 10 is used to update the guess for ${}_i{}^j\boldsymbol{V}$ until $\left|{}_i{}^j\boldsymbol{G}\right|$ is less than some tolerance.

$${}_i{}^j[DG]\Delta\boldsymbol{V} = \boldsymbol{0} - {}_i{}^j\boldsymbol{G} \tag{10a}$$

$${}_i{}^{j+1}\boldsymbol{V} = {}_i{}^j\boldsymbol{V} + \Delta\boldsymbol{V} \tag{10b}$$

Once $\left|{}_i{}^j\boldsymbol{G}\right|$ is less than some tolerance, ${}_i{}^*\boldsymbol{V}$ is set to ${}_i{}^j\boldsymbol{V}$, and the initial guess for the next member in the family is obtained by using Eq. 11.

$${}_i{}^*\hat{\boldsymbol{n}} = \mathrm{null}\left({}_i{}^*[DH]\right) \tag{11a}$$

$${}_{i+1}{}^0\boldsymbol{V} = {}_i{}^*\boldsymbol{V} + \Delta s_i \, {}^*\hat{\boldsymbol{n}} \tag{11b}$$

3.1.1 End of an orbit family

If the corrections scheme fails when computing a member of a family, the position and velocity elements of the state corresponding to the specified surface of section are examined. If the orbit member crosses the surface of section with a corresponding velocity component magnitude (i.e., $|\boldsymbol{v} \cdot \hat{\boldsymbol{s}}|$) less than some tolerance, the index and/or value of the surface of section is updated. If the corrections scheme fails to converge but this condition is not met, the previous orbit member is used to generate a new initial guess with a smaller step size Δs, and the corrections process is attempted again. This process is repeated until the next orbit member is successfully identified or until Δs falls below some tolerance.

The continuation algorithm is stopped if any of the following conditions are met: 1) Δs is smaller than an allowable limit, 2) the surface of section has been changed more times than a specified limit, 3) $|{}_i{}^*\boldsymbol{V} - {}_{i-1}{}^*\boldsymbol{V}|$ is greater than some tolerance, 4) the orbit corresponding to ${}_i{}^*\boldsymbol{V}$ matches an orbit that has been found previously, 5) i exceeds some specified limit, or 6) the corrections scheme fails and none of the adjustments listed previously are successful. If any of those conditions are met, careful consideration is needed to determine whether the family can be continued beyond that point by modifying the values of the continuation parameters. For example, if Condition 4 is met, additional analysis is needed to determine if this point corresponds to a reflection class accident or if the continuation algorithm failed to move past this point for some other reason. While every attempt was made to continue each family to its "true" termination condition, we cannot guarantee that we managed to identify the true "end point" of every family presented in this work.

Generally, once a member of an orbit family crosses the surface of a body, the computation of the family is stopped. The equations of motion used in this work (see Eq. 5) do not account for additional terms that influence motion inside the surface of the asteroid (e.g., internal pressure), so any orbit we obtain that crosses the surface of the asteroid is a non-physical result. The partial derivatives of the gravitational force potential cannot be evaluated at the surface of the asteroid in their current form (see Eq. 2) as a discontinuous change in the density of the body occurs at the surface (Tardivel 2014; MacMillan 1958). However, while periodic orbits that crossed the surface of the asteroid did take significantly longer to integrate and correct, computing these orbits was still possible even though the results were non-physical. Furthermore, as we do not have a reliable intuition for how these families behave, we cannot preclude the possibility that continuing the family further would eventually yield members that once again lie completely outside the surface of the asteroid. For that reason, we continue the families even after a member of the family crosses the surface of the asteroid.

3.2 Expected types of orbit families

As can be seen in Eq. 11, the computation of an orbit member relies on the previous member in the family. As a result, an initial orbit member is needed to start the continuation process. While we do not know all the possible orbit families that could exist, we do know how to obtain initial members for a few families.

3.2.1 Initial families

Far away from the asteroid, nearly circular orbits that lie close to the xy-plane should exist. These orbits correspond to the planar direct and retrograde families. An initial guess for both the planar direct and retrograde families was obtained using Eq. 12, where μ if the graviational parameter of the asteroid, $\beta_{\mathrm{P}} = -1$ for the direct family, and $\beta_{\mathrm{P}} = 1$ for the retrograde family (Scheeres 2012; Chappaz 2011).

$$ {}_{0}{}^{0}\boldsymbol{V} = \left[a_{\mathrm{P}} \; 0 \; 0 \; 0 \; -a_{\mathrm{P}}\dot{\theta}_{\mathrm{P}} \; 0 \; \frac{2\pi}{\dot{\theta}_{\mathrm{P}}} \right]^{T} \tag{12a} $$

$$ \dot{\theta}_{\mathrm{P}} = \omega + \beta_{\mathrm{P}} \sqrt{\frac{\mu}{a_{\mathrm{P}}^{3}}} \tag{12b} $$

a_{P} is the initial guess for the radius of the nearly circular orbit and should be sufficiently large so the orbit is far from the asteroid. These equations for the initial guess are based on Section 7.4.2 in Scheeres (2012). When correcting this initial guess, the constraint in $\boldsymbol{G}$ corresponding to the pseudo-arclength constraint was excluded (i.e., the last constraint in Eq. 9b was not included in the corrections scheme for this initial orbit). The position was constrained to lie in the xz-plane (i.e., $l_{\mathrm{PS}} = 2$ and $v_{\mathrm{PS}} = 0$). Once ${}_{0}{}^{*}\boldsymbol{V}$ was obtained by correcting the initial guess, the rest of the family was obtained by using the continuation algorithm.

Orbit families are also expected to exist around the equilibrium points. The Jacobian matrix was evaluated at each equilibrium point using Eq. 5c, and its eigenvalues were computed. For each pair of purely imaginary eigenvalues, there should be one orbit family emanating from that equilibrium point. Let the two eigenvalues $\lambda_{1,2} = \pm i\lambda_{\mathrm{O}}$ (where $\lambda_{\mathrm{O}} > 0$) and two eigenvectors $\boldsymbol{w}_{1,2} = \boldsymbol{w}_{a} \pm i\boldsymbol{w}_{b}$ correspond to one of these oscillatory modes. Let $\boldsymbol{X}_{\mathrm{EP}}$ represent the state of the equilibrium point where the Jacobian matrix was evaluated. First, the normalized vectors $\hat{\boldsymbol{w}}_{a}$ and $\hat{\boldsymbol{w}}_{b}$ are determined. Second, l_{PS} is set based on the largest velocity component of $\hat{\boldsymbol{w}}_{a}$ and $\hat{\boldsymbol{w}}_{b}$ (e.g., if the component corresponding to $\dot{z}$ is larger in magnitude than the components corresponding to $\dot{x}$ and $\dot{y}$, then $l_{\mathrm{PS}} = 3$). v_{PS} is then set to the corresponding position component of the equilibrium point based on l_{PS}. Finally, Eq. 13 is used to obtain an initial guess for the first orbit member on the family corresponding to this oscillatory mode.

$$ {}_{0}{}^{0}\boldsymbol{V} = {}_{-1}{}^{*}\boldsymbol{V} + \Delta s_{\mathrm{O}} \, {}_{-1}{}^{*}\hat{\boldsymbol{n}} \tag{13a} $$

$$ {}_{-1}{}^{*}\boldsymbol{V} = \begin{bmatrix} \boldsymbol{X}_{\mathrm{EP}} \\ \frac{2\pi}{\lambda_{\mathrm{O}}} \end{bmatrix} \tag{13b} $$

$$ {}_{-1}{}^{*}\hat{\boldsymbol{n}} = \begin{bmatrix} \delta\hat{\boldsymbol{X}}_{\mathrm{O}} \\ 0 \end{bmatrix} \tag{13c} $$

$$ \delta\boldsymbol{X}_{\mathrm{O}} = \hat{\boldsymbol{w}}_{a} + \left(-\frac{\hat{\boldsymbol{w}}_{a}^{l_{\mathrm{PS}}}}{\hat{\boldsymbol{w}}_{b}^{l_{\mathrm{PS}}}} \right) \hat{\boldsymbol{w}}_{b} \tag{13d} $$

Note in this equation $\delta\hat{\boldsymbol{X}}_{\mathrm{O}}$ represents the vector obtained by normalizing $\delta\boldsymbol{X}_{\mathrm{O}}$. Unlike initializing the planar families, all eight constraints in $\boldsymbol{G}$ (see Eq. 9b) are used to correct the initial member for these types of families. Note that the orbit corresponding to ${}_{-1}{}^{*}\boldsymbol{V}$ is not considered to be part of the orbit family, this notation is used simply to agree with the form of the terms in Eq. 9b. We use a Δs_{O} that is two orders of magnitude smaller than the value of Δs that is used for the other members in the family.

The two planar families and the families emanating from the equilibria will be referred to as “Initial Families” or “IFs.” When initialized far from the asteroid, the planar retrograde family and planar direct family will be referred to as OF-1-0 and OF-2-0, respectively. Bennu has eight equilibria on the ridge line, and these equilibria will be numbered one through eight

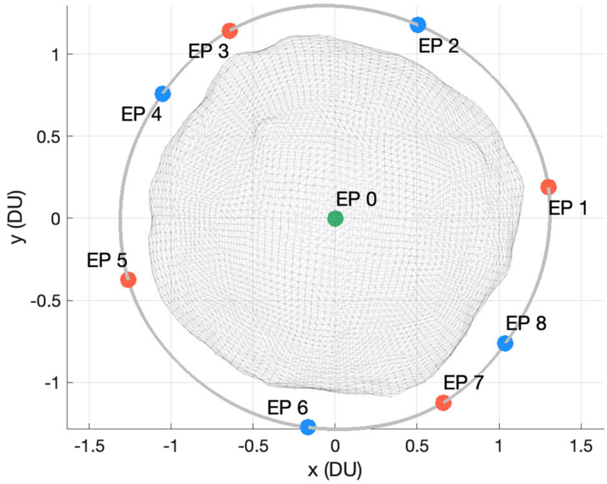

Fig. 1 Equilibria that exist around Bennu. Red dots correspond to saddles, blue dots correspond to unstable centers, and green dots correspond to stable centers. The gray line represents the ridge line

in ascending order of $\theta_{\mathrm{EP}} = \arctan\left(X^2_{\mathrm{EP}}/X^1_{\mathrm{EP}}\right)$ where $\theta_{\mathrm{EP}} \in [0, 2\pi)$ (Brown and Scheeres 2023b). EP 0 will refer to the one equilibrium point that lies inside the asteroid. The equilibria that exist around Bennu at its current spin rate are presented in Fig. 1 (Brown and Scheeres 2023b, a).

The terms used to describe the types of equilibria ("saddle," "unstable center," and "stable center") are defined to be consistent with Tardivel (2014). All of these equilibria have one 2-D center manifold corresponding to out-of-plane motion. A stable center has two additional 2-D center manifolds each corresponding to motion near the xy-plane, a saddle has one, and an unstable center has none (Tardivel 2014; Brown and Scheeres 2023b). One family is expected to emanate from an unstable center, two families are expected to emanate from a saddle, and three families are expected to emanate from a stable center. For EP i, OF-i-1 will refer to the family emanating from EP i with the most significant out-of-plane components (i.e., $\left|\delta X^6_{\mathrm{O}}\right| > \left|\delta X^4_{\mathrm{O}}\right|, \left|\delta X^5_{\mathrm{O}}\right|$). We expect that, of the up to three possible families that can exist around EP i, OF-i-1 will have the shortest period. The remaining families, if there are any, will have almost negligible out-of-plane components. If there is only one other family emanating from EP i, OF-i-2 will refer to this family. If there are two other families emanating from EP i, OF-i-2 will be the family with the smaller period of the two and OF-i-3 will be the other. For two different equilibria EP j and EP k, if OF-j-1 and OF-k-1 are actually the same family, this family will be referred to as OF-j/k-1.

3.2.2 Families identified from bifurcations in other families

In this paper, the phrase "bifurcation points" (or BPs) refers to points where the behavior or properties of an orbit family qualitatively change (Seydel 2010). Secondary-Hopf (SH), tangent (TB), and n-period (or nT) bifurcations are a few types of bifurcations we expect to encounter when continuing the orbit families. If we expect a bifurcation has occurred between two orbit members, we will use a bisection method to detect the bifurcation point with the criteria c_{BP} provided in Eq. 14 (Broucke 1969; Campbell 1999; Zimovan-Spreen et al. 2020).

$$c_{\mathrm{SH}} = B - \frac{1}{4}A^2 - 2 \tag{14a}$$

$$c_{\mathrm{TB}} = B - 2A + 2 \tag{14b}$$

$$c_{\mathrm{2T}} = B + 2A + 2 \tag{14c}$$

$$c_{\mathrm{3T}} = B + A - 1 \tag{14d}$$

$$c_{\mathrm{4T}} = B - 2 \tag{14e}$$

These criteria will have a value of zero when evaluated at a bifurcation point of the correct type, and are directly from Howard and MacKay (1987) and Campbell (1999). Please refer to those references for more information on these criteria. A and B are the stability parameters presented in Eq. 8. The bifurcation points will be labeled using the following notation: Family-i-j where "Family" is the name of the family that the bifurcation point was detected on. i indicates the type of bifurcation with $i = 0$ for Secondary-Hopf, $i = 1$ for tangent, and $i \geq 2$ for nT bifurcations where $n = i$. j indicates the number of bifurcations of that type that have occurred on the family up to and including the current bifurcation point. For example, 5-1-2-4 would refer to the fourth 2T bifurcation point identified on OF-5-1, and 1/2-1-1-2 would refer to the second tangent bifurcation point identified on OF-1/2-1 where the members of OF-1/2-1 are ordered with the member closest to EP 1 first and the member closest to EP 2 last.

Some of these points correspond to the intersection of two orbit families. The specific types of bifurcation points where we tried to compute additional families will be discussed in Sect. 4.2. The naming convention for these additional families, which will be referred to as "BFs," will also be discussed in that section. Let ${}_{\mathrm{BP}}{}^{*}\boldsymbol{V} = \left[{}_{\mathrm{BP}}{}^{*}\boldsymbol{X}^{T}\ {}_{\mathrm{BP}}{}^{*}T\right]^{T}$ be the orbit member corresponding to the bifurcation point on the "old" family. Equation 15, which is very similar to Eq. 13, is used to obtain a guess for an orbit on the "new" family.

$${}_{0}{}^{0}\boldsymbol{V} = {}_{-1}{}^{*}\boldsymbol{V} + \Delta s_{\mathrm{B}}\ {}_{-1}{}^{*}\hat{\boldsymbol{n}} \tag{15a}$$

$${}_{-1}{}^{*}\boldsymbol{V} = \begin{bmatrix} {}_{\mathrm{BP}}{}^{*}\boldsymbol{X} \\ n_{\mathrm{B}}\,{}_{\mathrm{BP}}{}^{*}T \end{bmatrix} \tag{15b}$$

$${}_{-1}{}^{*}\hat{\boldsymbol{n}} = \begin{bmatrix} \delta\hat{\boldsymbol{X}}_{\mathrm{B}} \\ 0 \end{bmatrix} \tag{15c}$$

$$\delta\boldsymbol{X}_{\mathrm{B}} = \hat{\boldsymbol{w}}_{a} + \left(-\frac{\hat{\boldsymbol{w}}_{a}^{l_{\mathrm{PS}}}}{\hat{\boldsymbol{w}}_{b}^{l_{\mathrm{PS}}}}\right)\hat{\boldsymbol{w}}_{b} \tag{15d}$$

In Eq. 15, $\hat{\boldsymbol{w}}_{a}$ and $\hat{\boldsymbol{w}}_{b}$ are normalized 6×1 real-valued vectors. These vectors are the full-state equivalent to the normalized 4×1 real-valued eigenvectors $\hat{\boldsymbol{y}}_{a}$ and $\hat{\boldsymbol{y}}_{b}$ corresponding to the mode of interest of the linearized Poincaré map $\left[\Phi_{M}^{\mathrm{R}}\right]$. $\hat{\boldsymbol{w}}_{a}$ and $\hat{\boldsymbol{w}}_{b}$ can be obtained from $\hat{\boldsymbol{y}}_{a}$ and $\hat{\boldsymbol{y}}_{b}$ by using Eq. 7a. The mode of interest is the mode of $\left[\Phi_{M}^{\mathrm{R}}\right]$ whose corresponding eigenvalue pair $\lambda_{1,2} = 1$ for tangent bifurcations, $\lambda_{1,2} = -1$ for period-doubling bifurcations, $\lambda_{1,2} = e^{\pm i2\pi/3}$ or $\lambda_{1,2} = e^{\pm i4\pi/3}$ for 3T bifurcations, and $\lambda_{1,2} = e^{\pm i\pi/4}$ or $\lambda_{1,2} = e^{\pm i3\pi/4}$ for 4T bifurcations (Campbell 1999). Also, n_{B} is set to the value of n for a nT bifurcation, or a value of 1 for all other bifurcation types. All eight constraints in $\boldsymbol{G}$ (see Eq. 9b) are used to correct the initial member on each of these families. Note that the orbit corresponding to ${}_{-1}{}^{*}\boldsymbol{V}$ is considered to be part of the new orbit family. l_{PS} and v_{PS} are unchanged from the values used when computing the old family. Similarly to Δs_{O}, we use a Δs_{B} that is two orders of magnitude smaller than the value of Δs that is used for the other members.

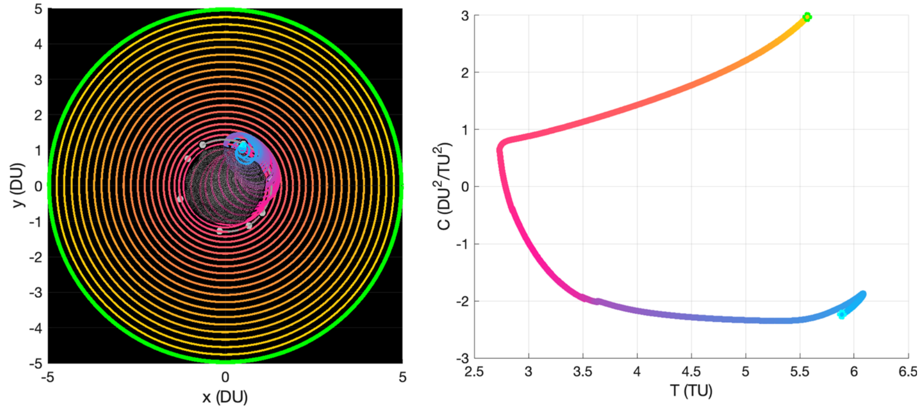

Fig. 2 Planar retrograde family (OF-1-0)

4 Numerical simulations

The set of orbits identified using this methodology will now be presented and the significant results will be discussed. The IFs will be presented first, starting with the IFs around EPs 3, 4, 7, and 8 as they appear to be similar. The direct and retrograde families will then be presented, followed by the IFs around EPs 1, 2, 5, and 6. The naming convention for these IFs was described previously in Sect. 3.2.1. Several BPs occur on these IFs that will result in new orbit families emanating from the IFs. These families will be referred to as "BFs." A table of all the BPs on the IFs will be presented. The set of BFs emanating from the IFs can be classified into four different types. The four BF types will then be presented.

The orbits identified using this model of Bennu will be compared to other simplified models, like the CR3BP and TAEM, to try to gain additional insight into why these orbit structures exist and behave in the way we have observed. When considering the comparisons to the CR3BP and TAEM, recall that in these models a Lyapunov orbit is a planar periodic orbit that emanates from an equilibrium point and a vertical orbit is an out-of-plane periodic orbit that emanates from an equilibrium point. Orbits that have potentially beneficial characteristics for spacecraft mission design will then be identified and the results will be discussed.

For the plots in this section, the yellow to pink to blue color scale indicates the progression along a family. The members in a family are indexed in an order where the "first" member is represented in green and the "last" member is represented in cyan. White lines in the position space plots and black circles in C vs T plots represent intersections of the family with orbit members on other families. Note that the intersection may correspond to a nT member on the other family.

4.1 Initial families

4.1.1 Direct and retrograde

The first members of the planar direct and retrograde families were computed using an initial guess of $a_P = 5$ DU. The retrograde family is represented in Fig. 2.

The first part of this family is shown in gold, orange, and pink. These members are nearly circular and very close to the xy-plane which is what we would expect. However, after this first

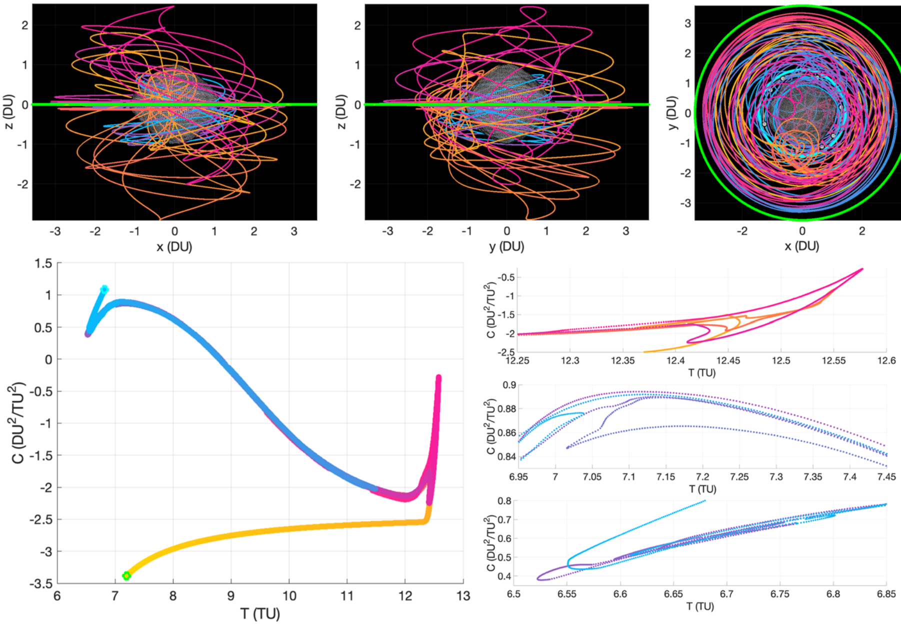

Fig. 3 Planar direct family (OF-2-0)

part, the family continues but shifts toward the first quadrant of the xy-plane, before ending at EP 2. It should be noted that the final members along this family match the members that would be obtained from OF-2-1. It should also be noted that orbit members with remarkably similar characteristics to the first part of this family can also be found inside the asteroid. These members were identified on the OF-5/0-2 family, but this will be discussed in more detail in Sects. 4.1.3 and 4.3.3.

The direct family is depicted in Fig. 3. To focus on the members closest to the asteroid, not all of the computed family members are shown. The first part (shown in gold in Fig. 3) is similar to what would be expected with nearly circular orbits that are very close to the xy-plane. The family then shifts out of the xy-plane. A few of the orbits are nearly symmetrical to other members in the family, and some parts of the family are nearly symmetrical to each other. There appear to be multiple portions of the family that have similar values of T and C. As will be covered in more detail in Sect. 4.3.1, these orbits have similar shapes as well, but are located in different regions of the phase space. This behavior is possibly a result of the fact that this asteroid does not have any symmetry in the exact sense, but it is nearly symmetric. OF-2-0 terminates at the orbit associated with the first 2T BP on OF-1-0.

4.1.2 IFs of EPs resulting from genesis events

As the spin rate of an asteroid changes, pairs of equilibria can come into existence together during “genesis events,” such as EPs 3 and 4 as well as EPs 7 and 8 (Brown and Scheeres 2023b). Both EP 7 and EP 8 have an eigenpair that should yield a “vertical” family. These families are OF-7-1 and OF-8-1. However, those families are connected to one another and contain the same members. Therefore, all the members in both of these families constitute one family, and this family will be referred to as OF-7/8-1. The same can also be said of

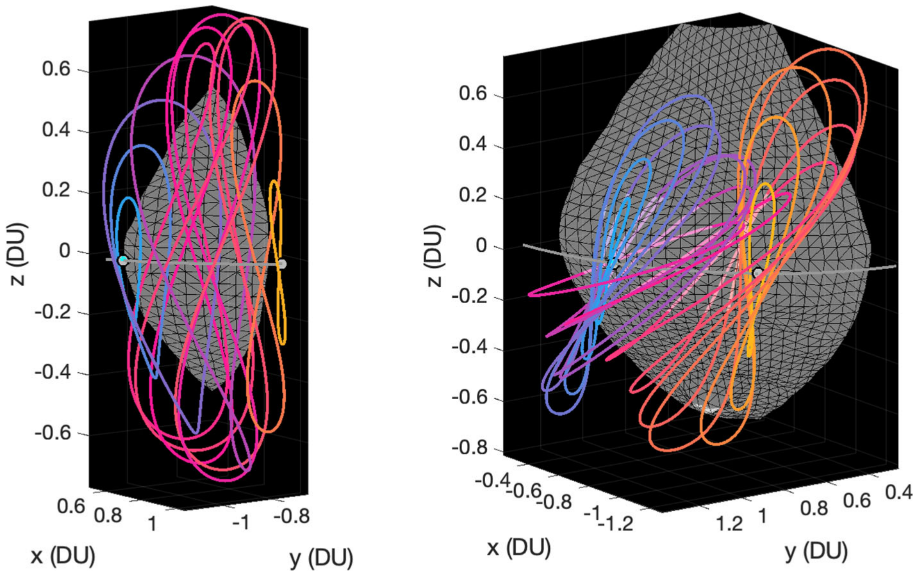

Fig. 4 OF-7/8-1 (left) and OF-3/4-1 (right) represented in configuration space

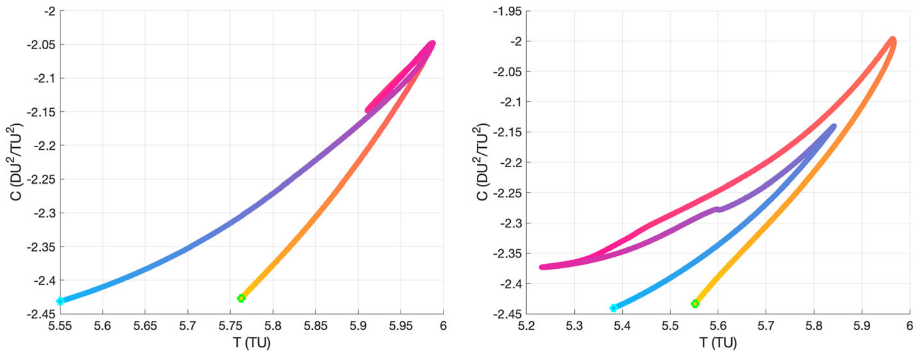

Fig. 5 OF-7/8-1 (left) and OF-3/4-1 (right) C vs T

EP 3 and EP 4. The "vertical" families emanating from those two EPs (OF-3-1 and OF-4-1) are actually one family that will be referred to as OF-3/4-1. OF-3/4-1 and OF-7/8-1 are represented in position space in Fig. 4, and their members' C and T values are presented in Fig. 5.

As can be seen in Figs. 4 and 5, the "vertical" families OF-3/4-1 and OF-7/8-1 are very similar. Near the EPs, the members of both families closely resemble the shapes of "vertical" orbits we have seen in the CR3BP (Doedel et al. 2007) and the TAEM (Romanov and Doedel 2012). However, farther away from the EPs, the orbit members in the "middle" of the family start to dip down toward the xy-plane. This feature is present in both OF-3/4-1 and OF-7/8-1, but it is far more pronounced in OF-3/4-1 than it is in OF-7/8-1. It should also be noted that no members of OF-7/8-1 penetrate the surface of the asteroid, while several members in the "middle" section of the OF-3/4-1 family do cross the asteroid's surface.

While we will not provide a general proof guaranteeing that the "vertical" families from two EPs originating from a genesis event are connected, we will present one possible explanation for this behavior. It should be noted that EPs 7 and 8 came into existence from a single degenerate equilibrium point at a lower spin rate than the current spin rate of the asteroid. At this singular point, the two eigenpairs with nonzero eigenvalues are those associated with the "vertical" and "Lyapunov" orbit families identified in this work (Brown and Scheeres 2023b). Let us say the spin rate is increased very slightly so that now two distinct EPs exist and the separation between them is very small. Under a few reasonable assumptions, as the spin rate is increased these eigenvalues and eigenvectors should evolve "smoothly." So, both EPs (at the slightly increased spin rate) should have an eigenpair that is nearly identical to one of the two nonzero eigenpairs of the degenerate EP (at the spin rate corresponding to the genesis event) (Brown and Scheeres 2023b). A "vertical" family can be computed about each of these EPs because there is an eigenpair corresponding to an oscillatory mode whose eigenvectors are primarily in the z and/or $\dot{z}$ directions. Both of these eigenpairs evolved from the same "vertical" eigenpair of the degenerate EP at the spin rate corresponding to the genesis event. With that in mind, it makes sense that these two families are connected to each other and, as a result, constitute one family. As the spin rate is increased further, the EPs move farther away from each other and the family continues to evolve. If no perturbations or other influencing factors have a significant enough effect to sever the connection, then this "vertical" family will continue to remain as one connected structure.

There were two other IFs identified from these two EP pairs, one from EP 3 (OF-3-2) and one from EP 7 (OF-7-2). These families can be seen in Figs. 6 and 7. No other orbit families can be obtained from the linearization about these EPs, so there are no other IFs emanating from these EPs.

In addition to the similarities between OF-3/4-1 and OF-7/8-1, we also see similarities between OF-3-2 and OF-7-2. Both OF-3-2 and OF-7-2 start from the second oscillatory mode associated with the saddle EP in each EP pair (EP 3 and EP 7). Before crossing the surface, the members of these two families (the gold portions in Figs. 6 and 7) look very much like "Lyapunov" orbits in the CR3BP (Doedel et al. 2007) and the TAEM (Romanov and Doedel 2012). After the surface is crossed, the behavior of the members changes slightly. In the gold to magenta portions, the vertical amplitudes of members on both families start to grow, before decreasing to almost negligible values. This feature is far more pronounced in OF-3-2, but it still is detected in OF-7-2. In the portion of both families that follows (the magenta to purple portions of OF-7-2 and the purple portions of OF-3-2), there is a minimal change in the shape and Jacobi energy of the orbit members, but there is a significant increase in their periods. It is at this point where the qualitative difference to the previous portions of the families becomes significant. The final portions of both OF-3-2 and OF-7-2 have members with significant vertical amplitudes. The families then terminate at the orbit associated with the 2T BP closest to the center EP along that EP pair's "vertical" family (i.e., OF-3-2 terminates at 4-1-2-1 and OF-7-2 terminates at 8-1-2-1). To reiterate, the last portions of OF-3-2 and OF-7-2 (the blue portions) consist entirely of orbits that would be obtained by computing the first parts of OF-4-1-2-1 and OF-8-1-2-1.

Focusing on OF-3-2, we expect that for a set of spin rates slightly larger than the spin rate corresponding to the genesis event for EP 3 and 4, a "Lyapunov" family would exist for EP 4 (OF-4-2) and for EP 3 (OF-3-2). Based on the discussion related to the "vertical" families, it might be expected that OF-3-2 and OF-4-2 would actually be one family OF-3/4-2. But unlike OF-3/4-1, which did not encounter changes that had a significant effect on its structure, the same cannot be said for OF-3/4-2. As identified in Brown and Scheeres (2023b), EP 4 transitions from a stable center to an unstable center, and loses the families corresponding

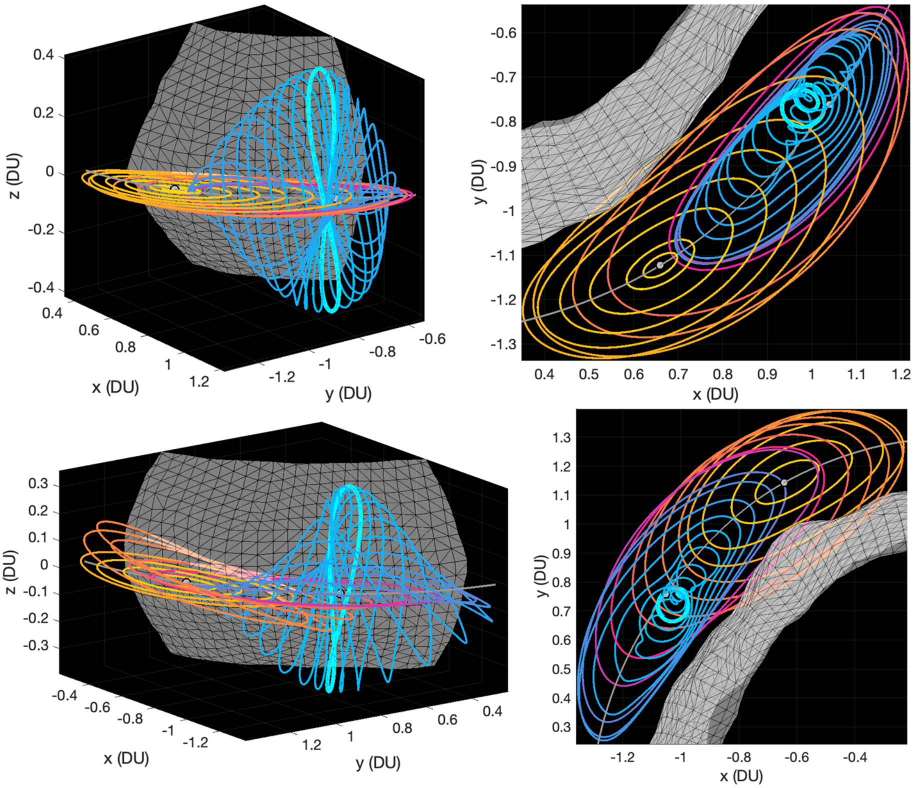

Fig. 6 OF-7-2 (top) and OF-3-2 (bottom) represented in configuration space

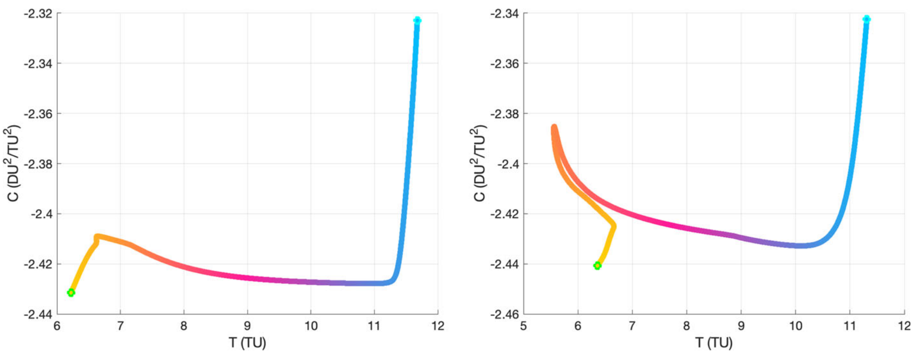

Fig. 7 OF-7-2 (left) and OF-3-2 (right) C vs T

to the second and third oscillatory modes it once had (OF-4-2 and OF-4-3). The eigenpair associated with OF-4-1 is not directly affected by this process as it involves a collision of the eigenpairs corresponding to OF-4-2 and OF-4-3. The structure of OF-3/4-2 that existed before this loss of stability cannot be directly reached from the linearization around EP 4 after this loss of stability. With this in mind, it is of interest to explore the manner in which the connection between EP 4 and OF-3/4-2 is broken. This process is shown in Fig. 8.

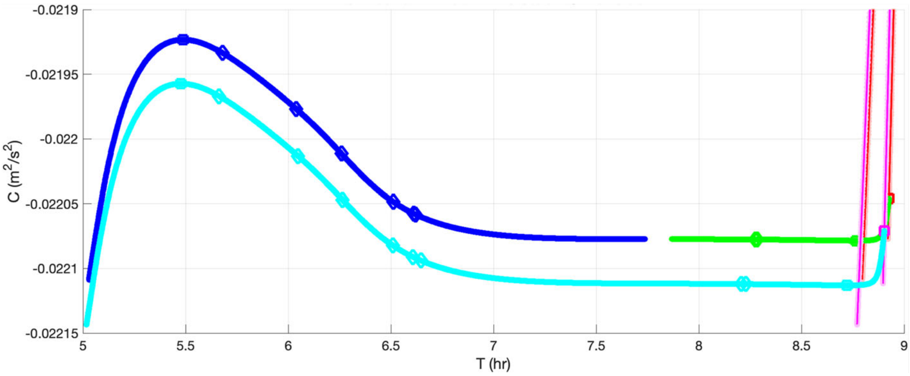

Fig. 8 IFs near EP 4's stability transition. In this caption, "before" will refer to the spin rate slightly slower than the stability transition spin rate and "after" will refer to the spin rate slightly faster than the stability transition spin rate. OF-3/4-1 (before is in red, after is in magenta), OF-3/4-2 (before is in blue), OF-4-3 (before is in green), OF-3-2 (after is in cyan). The squares and diamonds represent BPs on the IFs

At a spin rate just below the stability transition of EP 4, OF-4-3 starts at EP 4. Progressing along the family, the orbit members move away from EP 4, their periods increase, and their values of C decrease. A local minimum in C is then reached, and the family ends at a BP on OF-4-1. The members of OF-4-3 match the members that would be obtained by computing OF-4-1-2-1. At this same lower spin rate, if the computation of OF-3/4-2 is started at EP 3, as you progress along the family, the orbit members get closer to EP 4, their periods increase, and their values of C decrease. At a spin rate slightly higher than the spin rate corresponding to the stability transition of EP 4, the structures of OF-3/4-2 and OF-4-3 join together. However, instead of meeting at EP 4, they meet at some orbit that is farther away from EP 4. So, the connection to 4-1-2-2 was originally a part of the structure of OF-4-3, but after the stability transition of EP 4, the OF-3-2 structure "absorbs" that OF-4-3 structure. After this stability transition, while the structure of OF-3-2 remains similar in the vicinity of EP 3, it is qualitatively different in the vicinity of EP 4 as it now connects to 4-1-2-2. The same statements apply to the evolution of OF-7-2.

In summary, four distinct orbit families were determined from the linearization around the EPs that originated from a genesis event. One "vertical" family connecting EPs 7 and 8 (OF-7/8-1), one "Lyapunov" family originating from EP 7 (OF-7-2), one "vertical" family connecting EP 3 and 4 (OF-3/4-1), and one "Lyapunov" family originating from EP 3 (OF-3-2) were identified. Overall, the orbit structures of the IFs emanating from EPs 3 and 4 and the IFs emanating from EP 7 and 8 are very similar at the current spin rate. Furthermore, it seems that these structures evolve in similar ways and that the orbit structure around EPs 3 and 4 is more "evolved" than the orbit structure around EPs 7 and 8. In other words, we expect that the fundamental orbit structure that would exist around EPs 7 and 8 at a faster spin rate would more closely resemble the fundamental orbit structure that currently exists around EPs 3 and 4 at the current spin rate. We would expect this orbit structure to exist around all other EPs coming from genesis events (such as EPs 9 and 10 and EPs 11 and 12 identified in Brown and Scheeres (2023b), which exist at faster spin rates). While there could still be significant differences in the structures of the IFs as a result of local variations in the gravity field, we expect these structures to evolve in a similar manner.

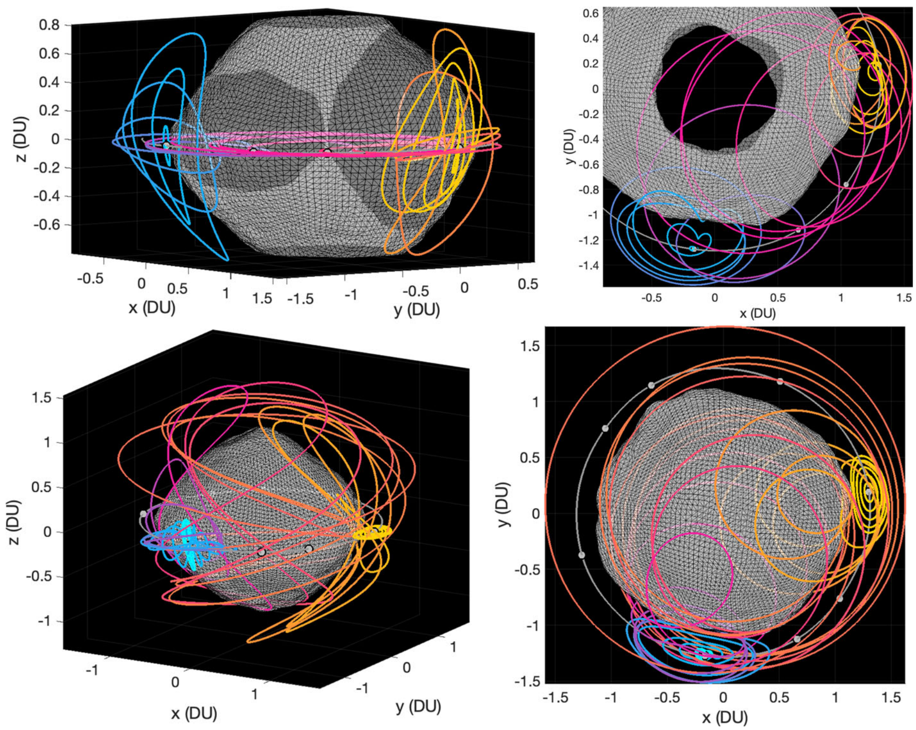

Fig. 9 OF-1/6-1 (top) and OF-1-2 (bottom) represented in configuration space

4.1.3 IFs of the original EPs

The remaining IFs all were generated from linearizations around EPs 1, 2, 5, and 6. These EPs will be referred to as the "original" EPs as they existed at the slowest spin rates studied in Brown and Scheeres (2023b). These four EPs are related to the four EPs detected outside the surface of the TAEM seen in Romanov and Doedel (2012) in terms of location and type. It is important to note that the evolution of these "original" EPs is fundamentally different from the EPs coming from genesis events. That being said, the IFs computed from the linearizations around EPs 1 and 6 are qualitatively similar to the families emanating from the EPs coming from genesis events. For that reason, the IFs around EPs 1 and 6 will be discussed first. We identified two IFs emanating from EPs 1 and 6: OF-1/6-1 and OF-1-2. These two IFs are presented in Figs. 9 and 10.

The "vertical" families starting at EPs 1 and 6 (OF-1-1 and OF-6-1) are actually one family that will be referred to as OF-1/6-1. The "middle" portion of the family lies almost entirely in the xy-plane. While the family around EP 1 includes more turning points, overall this family seems to have a structure that is consistent with the structure of OF-7/8-1 and OF-3/4-1. While the explanation for why the families from two different EPs were connected for OF-7/8-1 and OF-3/4-1 was based on how both EPs in the pair came from the same degenerate EP, this explanation obviously does not apply to EPs 1 and 6. So, it seems that there could be an underlying global effect that explains this type of connection between OF-1-1 and OF-6-1.

The "Lyapunov" family starting at EP 1 (OF-1-2) is also similar to OF-3-2 and OF-7-2. The most significant difference between OF-1-2 and those other two IFs is the vertical

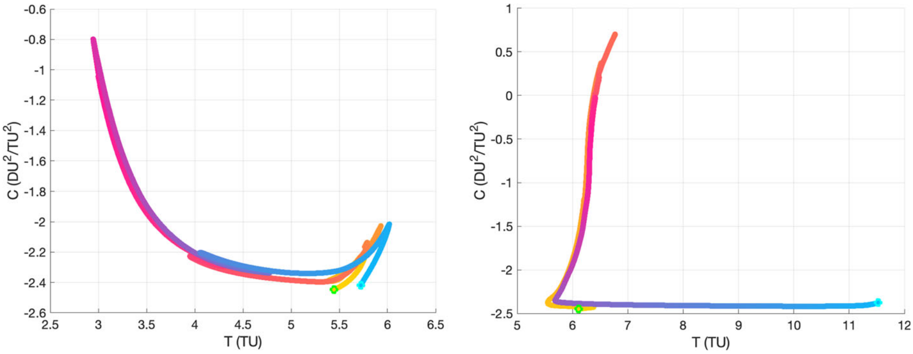

Fig. 10 OF-1/6-1 (left) and OF-1-2 (right) C vs T

amplitudes of members on OF-1-2 grow much larger after crossing the surface than the members on OF-3-2 and OF-7-2. In fact, this part of the family (the orange to light purple portions) develops to the point that the family members almost reach the xy-plane in a near circular shape about the asteroid. Except for that difference, the families are very similar qualitatively. Before crossing the surface (the gold portion), the members of OF-1-2 look like traditional "Lyapunov" family orbits seen in the CR3BP (Doedel et al. 2007) and the TAEM (Romanov and Doedel 2012). After the vertical amplitude of the orbits grows and returns to near zero (the orange to light purple portions), there is a portion of the family (the purple to dark blue portions) whose members have very similar shapes and Jacobi energies, but have a wide range of periods. The family then terminates at the orbit associated with the 2T BP closest to EP 6 on the "vertical" family OF-1/6-1 (i.e., OF-1-2 terminates at 6-1-2-1). Overall, it seems that the structure of the IFs around EPs 1 and 6 (OF-1/6-1 and OF-1-2) is consistent with the structure of the IFs around EPs 3 and 4 and EPs 7 and 8. It would seem that this structure of the IFs around EPs 1 and 6 is the most "evolved," followed by the structure of the IFs around EPs 3 and 4, followed by the structure of the IFs around EPs 7 and 8 which is the least "evolved."

The IFs emanating from the two remaining EPs (EPs 2 and 5) are depicted in Figs. 11 and 12. Based on the structure of the IFs associated with the other six EPs, one might expect the structure to be similar for these two EPs. However, there are significant qualitative differences in the structure of these IFs. For example, OF-2-1 and OF-5-1 are not connected. OF-2-1 initially develops in a similar way to OF-3/4-1, OF-1/6-1, and OF-7/8-1. However, once OF-2-1 returns to being very close to the xy-plane, it follows a different path than those three IFs, and the final portion of OF-2-1 (the blue portion) matches the members obtained on OF-1-0 (the retrograde family).

It is also interesting that the final portion of OF-5-2 (the blue portion) contains orbit members that very closely resemble the retrograde family if OF-1-0 continued into the interior of the asteroid instead of shifting toward EP 2. Only EPs on the ridge line have been considered up to this point in our analysis. However, there is one interior EP (EP 0) that exists very close to the origin at the current spin rate. It should be noted that the members in the final portion of OF-5-2 match the first members that would be obtained by computing OF-0-2. For this reason OF-5-2 and OF-0-2 will be referred to as OF-5/0-2.

Before the first surface crossing OF-5-1 is similar to OF-1/6-1, OF-3/4-1, and OF-7/8-1. Even immediately after the first surface crossing, the structure of OF-5-1 is similar to the structure of OF-1/6-1. However, at some point, it seems that OF-5-1 and OF-5/0-2 switch

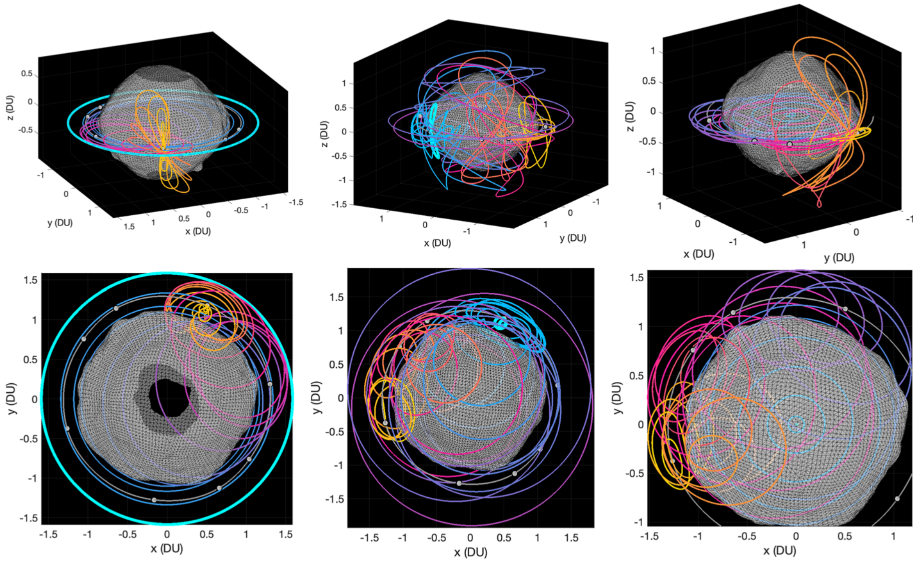

Fig. 11 OF-2-1 (left), OF-5-1 (middle), and OF-5/0-2 (right) represented in configuration space

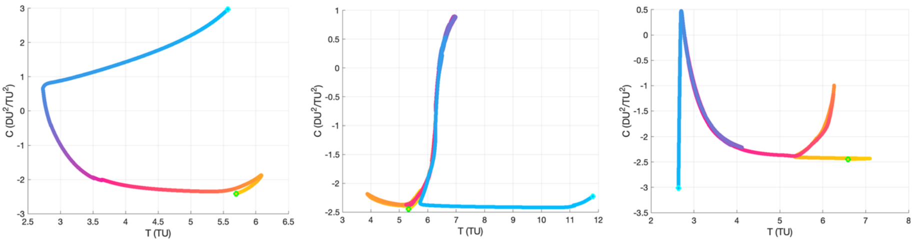

Fig. 12 OF-2-1 (left), OF-5-1 (middle), and OF-5/0-2 (right) C vs T

the path we would expect them to be on. For example, the "middle" part of OF-5-1 remains far outside the xy-plane unlike the "middle" parts of OF-1/6-1, OF-3/4-1, and OF-7/8-1, but more closely resembling the "middle" parts of OF-1-2, OF-3-2, and OF-7-2. In addition, the "middle" part of OF-5/0-2 returns to being almost entirely in the xy-plane unlike the "middle" parts of OF-1-2, OF-3-2, and OF-7-2, but closely resembling the "middle" parts of OF-1/6-1, OF-3/4-1, and OF-7/8-1. Furthermore, OF-5-1 terminates at the orbit associated with the 2T BP closest to EP 2 on the "vertical" family OF-2-1, which is very similar to the terminations of OF-1-2, OF-3-2, and OF-7-2. We do not know if this feature persists for these families at all spin rates. It is possible that these features are observed in these particular IFs even at the slowest spin rates. However, it is also possible that at a lower spin rate: 1) OF-2-1 and OF-5-1 would be connected and that family (OF-2/5-1) would more closely resemble OF-1/6-1, and 2) OF-5-2 would more closely resemble OF-1-2. Additional study is needed to determine the behavior of these families at slower spin rates.

It is also notable that analysis was performed in Brown and Scheeres (2023a) that concluded if the spin rate of Bennu was increased far beyond the current spin rate, EP 1 would annihilate with EP 0, EP 5 would annihilate with EP 6, and EP 2 would persist. While identifying EP pairs originating from genesis events provided insight into what IFs would be

Table 1 BPs on IFs used to generate BFs

IF	SH BPs	2T BPs	3T BPs	4T BPs
1/6-1	6-1-0-1 (297)	6-1-2-1 (297) 6-1-2-2 (692) 6-1-2-3 (1027)	6-1-3-1 (350)	6-1-4-1 (462)
1-2	–	–	–	–
2-1	2-1-0-1 (508)	2-1-2-1 (661) 2-1-2-2 (699) 2-1-2-3 (1247)	2-1-3-1 (522)	2-1-4-1 (628)
3/4-1	4-1-0-1 (447)	4-1-2-1 (447) 4-1-2-2 (664) 4-1-2-3 (1189)	4-1-3-1 (490)	4-1-4-1 (589)
3-2	–	–	–	**3-2-4-1 (457)**
5-1	–	–	–	–
5-2	–	–	**5-2-3-1 (534)**	**5-2-4-1 (145)**
7/8-1	8-1-0-1 (437)	8-1-2-1 (468) 8-1-2-2 (530)	8-1-3-1 (447) 8-1-3-2 (711)	8-1-4-1 (513) 8-1-4-2 (829)
7-2	–	–	–	–

Note that only the BPs that occurred before the first surface crossing are included in this table. Also note that BPs corresponding to tangent bifurcations are not included. The number in parentheses indicates the index of the orbit member on the IF that is closest to the BP. For OF-1/6-1, OF-3/4-1, and OF-7/8-1, the first number in the BP indicates which EP served as the reference for the index in parentheses (e.g., OF-6-1-2-3 is the third 2T BP detected on OF-1/6-1 when starting that IF at EP 6). Bold entries indicate a BF could not be generated at that BP due to numerical issues

connected, knowing which of these original EPs annihilate with each other did not. Overall, there appears to be a similar orbit structure in the IFs that connect pairs of EPs. As the spin rate changes, this structure involving each EP pair "evolves." At the current spin rate, each of these structures exhibit some unique behavior. However, there are enough similarities to assert that these orbit structures "evolve" in a similar manner.

4.2 Families identified from bifurcations in the initial families

The next group of orbit families were computed from BPs along each IF. To limit the number of computed families, BFs were only computed at the BPs along each IF that occurred before the IF crossed the surface for the first time. In the cases where a family starts and ends at two different EPs (OF-1/6-1, OF-3/4-1, and OF-7/8-1), the BPs that occurred before the first crossing when starting the IF from both EPs were included. It should be noted that a few BPs corresponding to tangent bifurcations were detected along these portions of the IFs, but no BFs could be continued from these BPs using our algorithm. A list of all BPs that were used to compute the BFs is provided in Table 1. Note that the naming convention for these BPs was described previously in Sect. 3.2.2.

The BPs corresponding to Secondary-Hopf bifurcations are included in Table 1 but generally could not be used to generate other families (Campbell 1999). However, it should be noted that the BPs 4-1-0-1 and 6-1-0-1 appear to correspond to Krein collisions that occur very close to the strong resonance of $\lambda^2 = 1$ (where λ is an eigenvalue of the IF orbit's monodromy matrix). Similarities in the way bifurcations occur along the IFs alludes to the similarities in the overall structure of the IFs. Almost no BPs were detected along the portions

Table 2 BPs in each BF

BFs	BPs				
A EP 2	2-1-2-2	2-1-3-1	5-1-2-2		
A EP 4	4-1-2-2	4-1-3-2	4-1-4-1	4-1-5-?	
A EP 6	6-1-2-2	6-1-3-2	6-1-4-1	6-1-5-?	(6-1-2-2)-2-4
A EP 8	8-1-2-2	8-1-3-1	7-2-2-4		
B EP 8	7-2-2-1	8-1-3-2	7-2-3-1	8-1-4-2	(8-1-2-2)-2-6
C EP 2	2-1-4-1				
C EP 4	4-1-3-1				
C EP 6	6-1-3-1				
C EP 8	8-1-4-1	7-2-3-2	(8-1-2-2)-2-1		
D EP 2	2-1-2-3	2-1-2-4			
D EP 4	4-1-2-3	4-1-2-4			
D EP 6	6-1-2-3	6-1-2-6			

The name of each BF is the first BP listed in each row in this table. It should be noted that some of these BFs passed through bifurcation points that were associated with other BFs, not IFs. In these cases, the other BF that the BP was detected on replaces the IF information when presenting the BP information (e.g., (8-1-2-2)-2-1 indicates the first 2T BP identified on OF-8-1-2-2 when starting that BF at the member closest to 8-1-2-2). Note that the order of the 5T BPs on OF-4-1 and OF-6-1 were not computed

of the IFs closest to the saddle EPs. Even the BPs that were detected close to these saddle EPs could not be used to generate a BF due to numerical computation issues.

The algorithm used to compute the BFs was continued until a termination condition was reached. When continuing the BFs away from the orbit corresponding to the original BP, some of the BFs actually contain members corresponding to other BPs on the IFs. Patching these branches that connect different BPs together can create a continuous orbit structure. Table 2 shows the BPs that were connected to form the complete BFs.

For the remainder of this paper, “BFs” will refer to these “complete” orbit structures. Four types of BFs were detected and they will be referred to as Types A, B, C, and D. Overall, 12 distinct BFs were identified from the 21 BPs in Table 1. Many of the BPs occur along the IFs close to the center EPs. For this reason the type of the BF and the center EP which the BF is closest to in phase space is provided in Table 2. Every attempt was made to ensure that the BFs could not be continued beyond the start and end points specified in Table 2. However, we cannot guarantee that all of these BFs cannot be continued beyond the endpoints specified in this table.

If the BF is “open” (if the continuation algorithm terminates at a different BP than the BP where it started) and the two BPs where the BF starts and ends are of the same type and belong to the same IF (e.g., a BF that starts at 4-1-2-3 and ends at the 4-1-2-4), the BF will be given the same name as whichever of the two BPs was identified first on that IF (e.g., in the previous example that BF would be named OF-4-1-2-3). If the BF is “open,” and the BPs where the BF starts and ends are not of the same type and/or do not belong to the same IF, the BF will be given the same name as whichever of the two BPs has the smallest period. For example, say a BF is comprised of a set of branches that when connected together starts at 8-1-2-2, passes through 8-1-3-1, and ends at 7-2-2-4. If the BF has a smaller period near 8-1-2-2 than it does near 7-2-2-4, this BF will be referred to as OF-8-1-2-2. If the BF is “closed” (if the continuation algorithm terminates at the same BP as the BP where it started) and the BF contains a BP on a “vertical” IF, the BF will be given the same name as that BP.

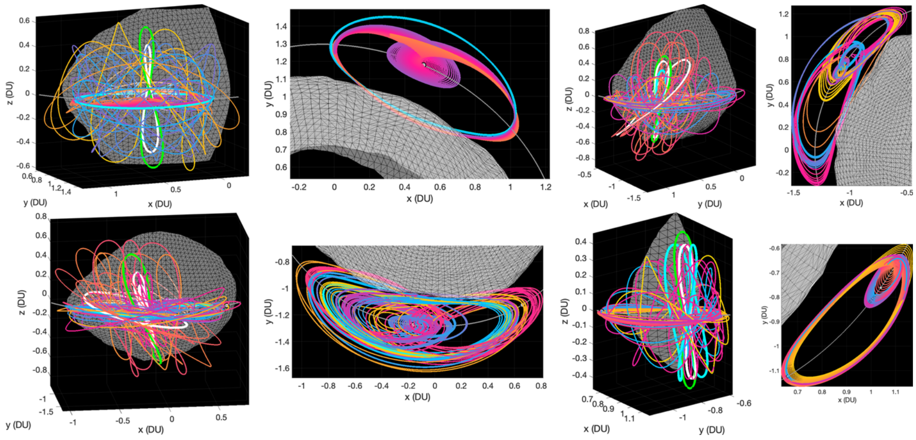

Fig. 13 BF Type A (OF-2-1-2-2, OF-4-1-2-2, OF-6-1-2-2, and OF-8-1-2-2) represented in configuration space. In this caption, "planar members" are orbits with z amplitudes less than a specified value (∼0.1 DU). Each family has two plots. From left to right then top down: OF-2-1-2-2 all members then planar members, OF-4-1-2-2 all members then planar members, OF-6-1-2-2 all members then planar members, OF-8-1-2-2 all members then planar members

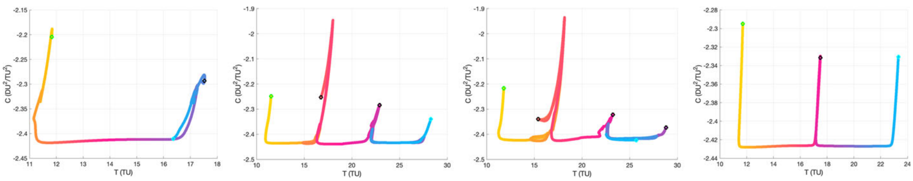

Fig. 14 BF Type A (from left to right: OF-2-1-2-2, OF-4-1-2-2, OF-6-1-2-2, and OF-8-1-2-2) C vs T

This procedure for naming the BFs is not generally applicable to all BFs that could possibly be identified, but it is sufficient for all the BFs identified in this work. Note the terms "open" and "closed" are used slightly differently in this section than how they are used in Hénon (1997). Using this naming convention, the first BP listed in each row of Table 2 is the name of each complete BF.

4.2.1 BF Type A

The first type of BF identified in the results is Type A. One BF of this type was detected in the vicinity of each of the four center EPs (OF-2-1-2-2, OF-4-1-2-2, OF-6-1-2-2, and OF-8-1-2-2). These BFs are depicted in Figs. 13 and 14.

All four of these BFs start at the second 2T BP along each "vertical" family starting at the center EP. The first parts of these BFs are expected to connect to the remnants of OF-2-3, OF-4-3, OF-6-3, and OF-8-3 that existed when those four EPs were stable centers. While all four of those EPs are now unstable centers, the remnants of those families still exist at the current spin rate. These BFs then continue and connect to other BPs of different types. The "cleanest" example of this structure can be seen in OF-8-1-2-2. Of these four BFs, OF-8-1-2-2 is the only one that does not cross the surface. Also, the second flat part in the C vs T plot for 8-1-2-2 in Fig. 14 (purple to dark blue portion) seems to be a continuation of the first flat part in the same plot (orange to pink portion). This finding will be discussed more in

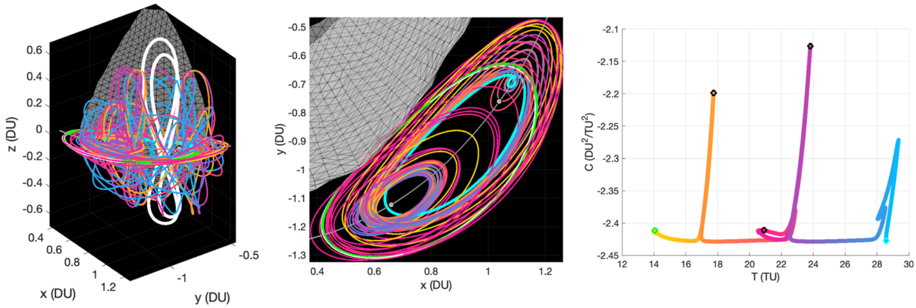

Fig. 15 BF Type B (OF-7-2-2-1)

Sect. 4.3.2. Some of these BFs contain parts that are not seen in all Type A BFs. For example, parts resembling the orange portions of OF-4-1-2-2 and OF-6-1-2-2 just after $T = 15$ TU in Fig. 14 are not seen in OF-6-1-2-2 or OF-8-1-2-2. However, the overall structure of these BFs is similar. Based on the similarities between some parts of these BFs and the structure of the other types of BFs, we expect that as these families "evolve," parts of these families may be "absorbed" by other BFs and/or some of these families may "absorb" other types of BFs.

The most similar BFs of this type are OF-4-1-2-2 and OF-6-1-2-2. The most significant difference between these two is that while OF-6-1-2-2 could be continued on the other side of the identified 5T BP on OF-6-1, OF-4-1-2-2 could not be continued on the other side of the identified 5T BP on OF-4-1. It is interesting to note that the endpoint for OF-6-1-2-2 was determined to be a 2T BP on itself. The endpoint for OF-8-1-2-2 was determined to be a 2T BP on OF-7-2 (7-2-2-4). However, the latter part of OF-7-2 includes members that have significant z amplitudes as OF-7-2 ends at 8-1-2-2. As can be seen in Fig. 13, the member of OF-7-2 corresponding to 7-2-2-4 is very close in phase space to some members of OF-8-1. Also, the period corresponding to 7-2-2-4 is very similar to three times the period corresponding to the orbits on OF-8-1 that are close to this BP. So, OF-4-1-2-2 and OF-8-1-2-2 both start and end at BPs that are either on or very near to the "vertical" family starting at the corresponding center EPs. OF-2-1-2-2 and OF-6-1-2-2 end at BPs where the corresponding orbits have almost no vertical component. It is important to note that all the BPs contained in these BFs, except for the BPs corresponding to the endpoints of OF-2-1-2-2 and OF-6-1-2-2, have a significant vertical component.

4.2.2 BF Type B

The next type of BF identified will be referred to as Type B. Only one BF of this type was detected (OF-7-2-2-1), and it is depicted in Fig. 15.

With regard to the similarities between Type A and Type B BFs, the "middle" portion of OF-7-2-2-1 bears a remarkable resemblance to the "middle" portions of OF-4-1-2-2 and OF-6-1-2-2. For example, the orange portions of OF-4-1-2-2 and OF-6-1-2-2 just after $T = 15$ TU in Fig. 14 are very similar to the pink portion of OF-7-2-2-1 in Fig. 15. The most significant difference between these two types is that both endpoints and one of the BPs in the middle of OF-7-2-2-1 are BPs whose corresponding orbits have virtually no vertical amplitude. It is this difference that led us to classify OF-7-2-2-1 as a different type of BF than OF-2-1-2-2, OF-4-1-2-2, OF-6-1-2-2, and OF-8-1-2-2, even though OF-7-2-2-1 is very similar to those Type A BFs. It is also interesting to note that the branches of this family

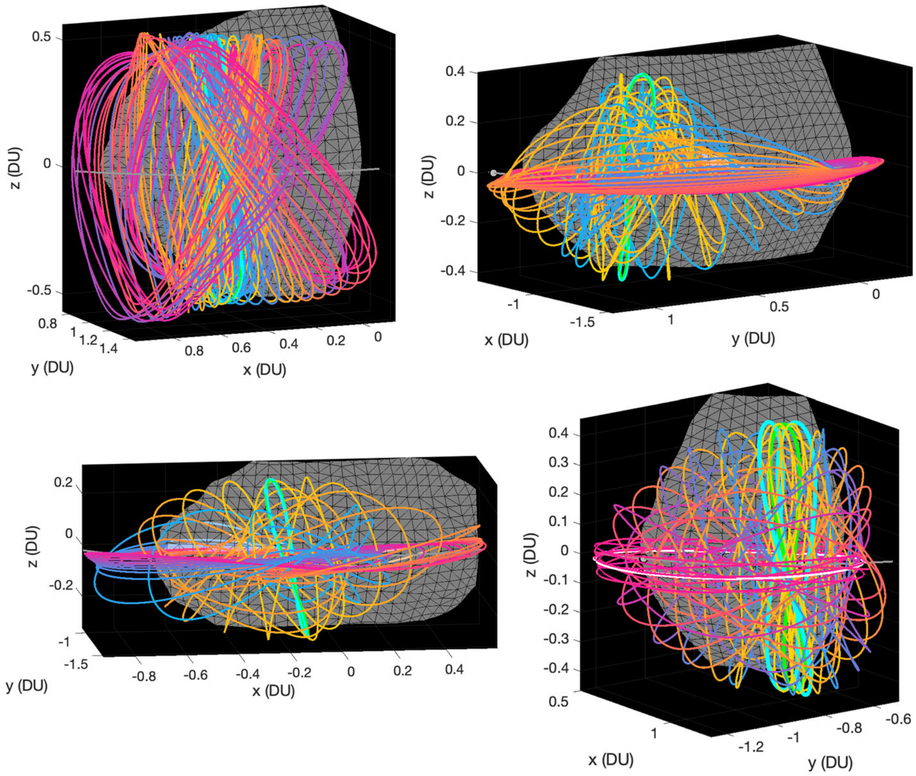

Fig. 16 BF Type C (from left to right then top down: OF-2-1-4-1, OF-4-1-3-1, OF-6-1-3-1, and OF-8-1-4-1) represented in configuration space

connecting 7-2-2-1 to 7-2-3-1 (gold through magenta portions) is very similar to the part of this family starting at 7-2-3-1 up until the family turns around at about $T = 28.05$ TU and $C = -2.394$ DU^2/TU^2 in the C vs T plot (magenta through dark blue portions) in Fig. 15. This feature will be discussed later in Sect. 4.3.1.

4.2.3 BF Type C

The third type of BF identified was Type C. These BFs are represented in Figs. 16 and 17.

The four BFs that are classified as this type are OF-2-1-4-1, OF-4-1-3-1, OF-6-1-3-1, and OF-8-1-4-1. Unlike Types A and B, Type C does not have parts where there are very little changes in C but large changes in T along the family. Of the four families of this type that were identified in the results, three begin and end at the same point. The fourth (OF-8-1-4-1) ends at the first 2T BP on OF-8-1-2-2. However, the orbit corresponding to this BP is very "close" to the orbit corresponding to the starting point in terms of T, C, shape, and other characteristics. It is also interesting that there is a BP on OF-8-1-4-1 that corresponds to a 3T BP on OF-7-2. The orbit on OF-8-1-4-1 corresponding to that BP can be viewed as a "midpoint" of this BF. Except for the start and end points of this family, the members on one side of the midpoint and the members on the other side of the midpoint are nearly symmetrical.

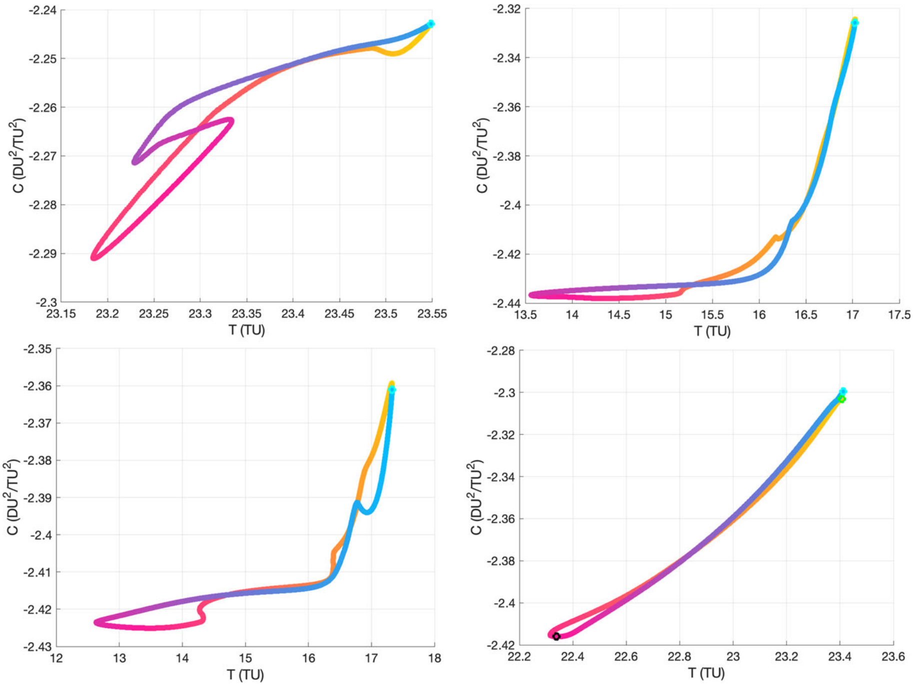

Fig. 17 BF Type C (from left to right then top down: OF-2-1-4-1, OF-4-1-3-1, OF-6-1-3-1, and OF-8-1-4-1) *C* vs *T*

While OF-2-1-4-1, OF-4-1-3-1, and OF-6-1-3-1 have members that are very similar to the members of the corresponding "Lyapunov" families, there is not a direct connection via a BP along the families. We expect that there may be a direct connection between these Type C BFs and the "Lyapunov" families at different spin rates, but these three families have "evolved" and that connection has been broken. While for these three families there is not a BP that can be viewed as a "midpoint" of the family, the first part and second part of these families are nearly symmetrical, although it is less distinctive than it was for OF-8-1-4-1. BFs of this type may be absorbed by Type A or Type B BFs as the spin rate changes. In addition, a structure that resembles a Type C BF, but is part of a Type A or Type B BF at a particular spin rate, may detach from the Type A or Type B BF and become its own distinct Type C BF as the spin rate varies. Particularly in the orange portions of OF-4-1-2-2 and OF-6-1-2-2 (Fig. 14) and in the magenta portion of OF-7-2-2-1 (Fig. 15), we see structures resembling Type C BFs.

4.2.4 BF Type D

The fourth and final type of BF identified in the results was Type D. The three BFs that were classified as Type D BFs (OF-2-1-2-3, OF-4-1-2-3, and OF-6-1-2-3) are represented in Fig. 18.

All three of these BFs start on a 2T BP on a "vertical" IF and end at another 2T BP on the same IF. The progression of C vs T along these three BFs is very similar to the progression of C vs T along the parts of the "vertical" IFs that are close to those BPs. We expect that BPs corresponding to the start and end of these BFs initially start as a single BP on their respective IF. It should be noted that the starting points of these BFs correspond to orbits

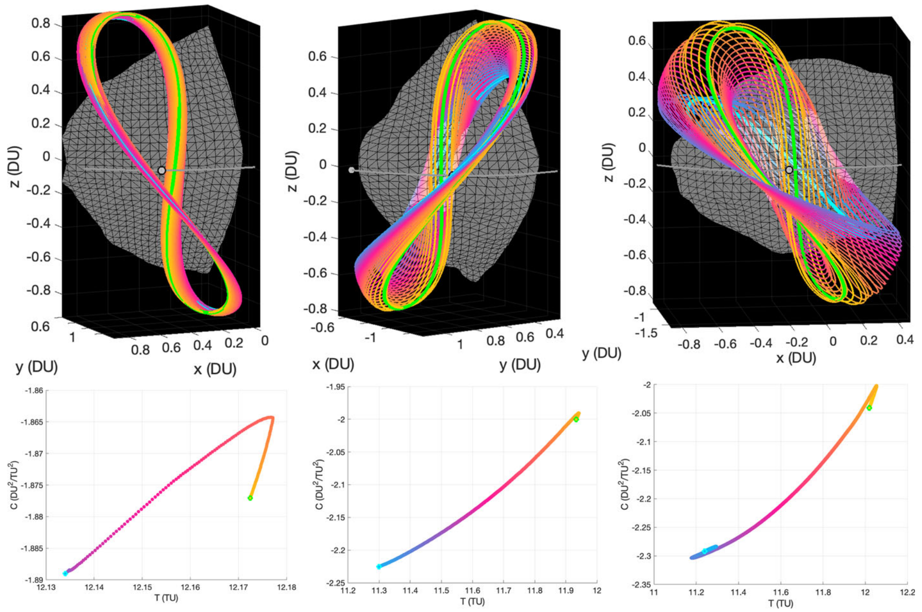

Fig. 18 BF Type D (OF-2-1-2-3 (left), OF-4-1-2-3 (middle), and OF-6-1-2-3 (right))

that are very close to the surface of the asteroid at some points, but remain entirely outside the surface. The orbits corresponding to the endpoints of these BFs are very similar, but they have portions that lie just inside the surface. As all members of OF-8-1 lie entirely outside the surface of the asteroid, this feature could be one reason why no BF of this type was identified in the vicinity of EP 8. If the spin rate increases beyond the point where some members of OF-8-1 cross the surface of the asteroid, we expect a Type D BF to develop in the vicinity of EP 8.

4.3 Other findings and similarities to other models

4.3.1 Nearly symmetric and symmetrical structures

While there is no perfect symmetry in the gravity field, there still appears to be some aspects of near symmetry in the orbit families around this asteroid. One example of this near symmetry is seen in the orbits computed starting at 8-1-2-1 (which are actually members of OF-7-2) and 8-1-2-2, and is presented in Fig. 19.

The members of these two groups of orbits seem to be both nearly symmetric about the xy-plane and nearly symmetrical to each other. However, they are not perfectly symmetric. Furthermore, the initial and final orbits of these groups are not the same. The orbits in these groups that lie near the xy-plane also appear to be nearly symmetric about the hz-plane (where the $\hat{\boldsymbol{h}}$ direction is evaluated at the center EP of interest and corresponds to the direction of $\boldsymbol{r}_{\text{EP}}$ projected into the xy-plane). This property of being nearly symmetric was also seen in 1) the orbits computed starting at 2-1-2-1 (members of OF-5-1) and 2-1-2-2, 2) the orbits computed starting at 4-1-2-1 (members of OF-3-2) and 4-1-2-2, and 3) the orbits computed starting at 6-1-2-1 (members of OF-1-2) and 6-1-2-2. However, in these groups of orbits,

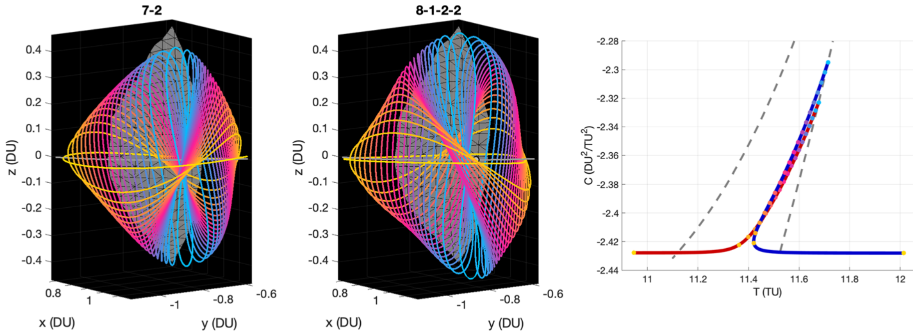

Fig. 19 Symmetries identified in orbits computed from 8-1-2-1 (members of OF-7-2) and 8-1-2-2. Orbits computed from the relevant BP on OF-8-1 up to the first local minimum in C are shown for both groups of orbits. In the C vs T plot, the dashed gray line represents part of OF-8-1 with its members' periods multiplied by two. The dark red solid line is the part of OF-7-2 near 8-1-2-1 and the dark blue solid line represents the orbits on BF-8-1-2-2 that are closest to 8-1-2-2

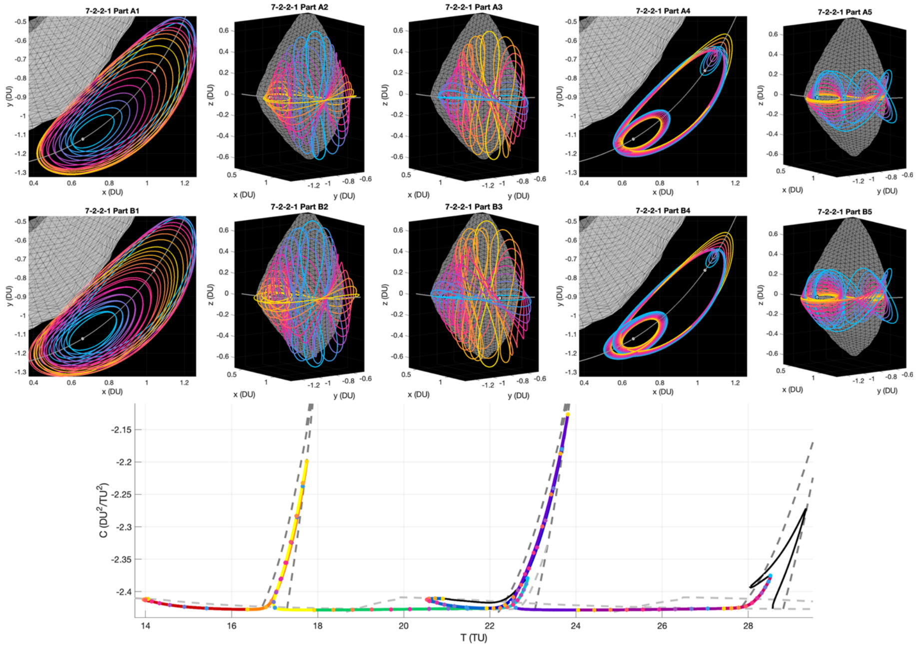

Fig. 20 Symmetries identified in OF-7-2-2-1. The order of the colors in the C vs T plot correspond to the parts shown in the top two rows. Dark red to teal corresponds to Parts A1-A5. Blue to red-violet corresponds to Parts B1-B5. In the top two rows, the ridge line is depicted by the gray line

the symmetry is not as obvious as it is for the orbits computed starting at 8-1-2-2 and the members of OF-7-2 near 8-1-2-1. There were also symmetries identified in members of the same family. For example, OF-7-2-2-1 consists of two main parts and is depicted in Fig. 20.

The first part (Part A) is represented by the dark red to teal portions in the C vs T plot which correspond to Parts A1-A5. Part A is very similar to the second part (Part B), which is represented by the blue to red-violet portions in the C vs T plot (Parts B1-B5). The primary difference between these two parts is that each orbit in Part B appears to have an extra loop

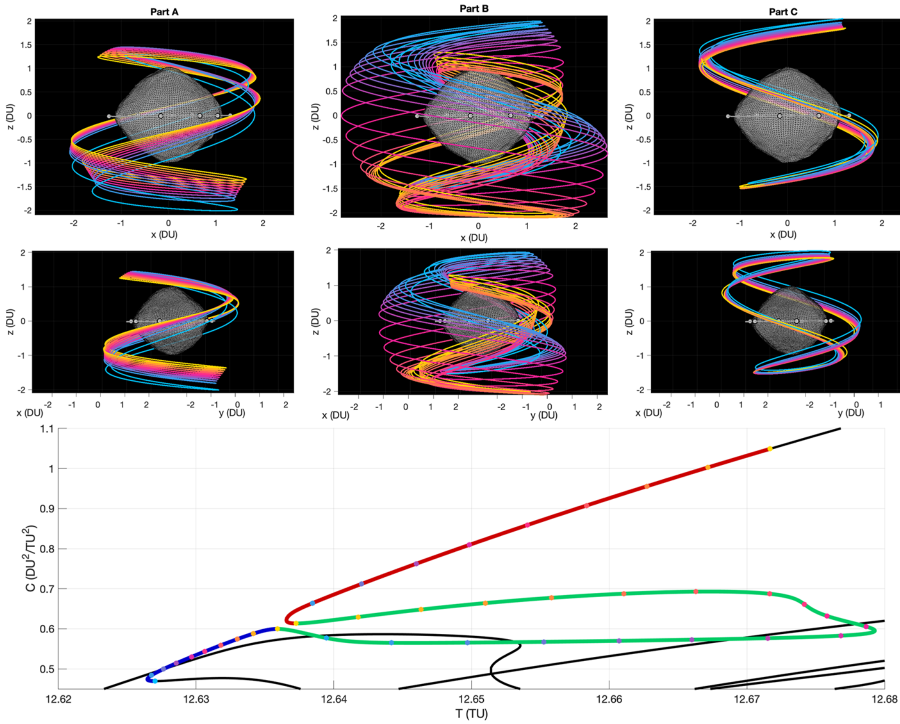

Fig. 21 Symmetries identified in OF-1-0-3-1. The order of the colors in the C vs T plot correspond to the individual parts shown in the top two rows. Red, green, and blue correspond to Parts A, B, and C, respectively

in the vicinity of EP 7, while the rest of the orbit appears relatively unchanged from its most similar counterpart orbit in Part A (e.g., the orbits in Parts A5 and B5). Similarly to the orbit groups in Fig. 19, Parts A2 and A3 and Parts B2 and B3 are nearly symmetric. Also, splitting this family into Part A and Part B is not the only way this family can be discretized into parts that appear to progress in the same way. By breaking down this family into more than two parts, it is possible to see more similarities to the structures present in the Type A BFs shown in Figs. 13 and 14.

There were also some members of OF-1-0-3-1 that were nearly symmetric. While the orbit families bifurcating off the retrograde and direct families were computed, most will not be presented in this paper. However, this particular BF will be briefly discussed here as it is relevant to the discussion of near symmetries. The relevant parts of this family are shown in Fig. 21.

Based on their shape in the configuration space, Parts A and C appear to be both nearly symmetric and nearly symmetrical to each other. That being said, the states on the orbits in these two parts appear to be far away from each other in the state space, even though they have very similar periods and Jacobi energies. Both Parts A and C comprise of members exclusively from OF-1-0-3-1. These two parts are connected to each other by the orbit members in Part B which also comprises of members from OF-1-0-3-1. It is possible that this Part B structure exists in this model simply to serve as a connection between two groups of orbits which are nearly symmetric in the same way. In other words, we are unsure if an orbit structure like

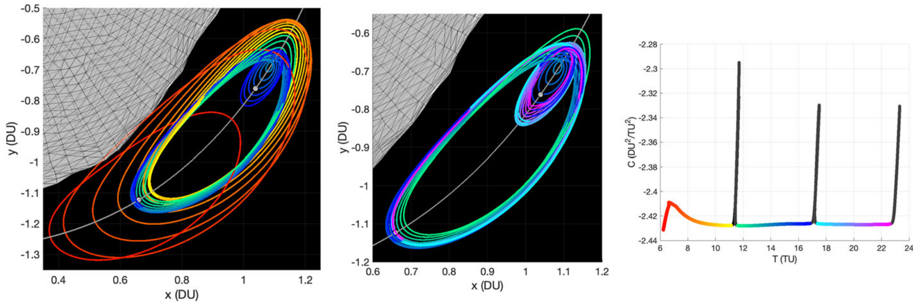

Fig. 22 Near connections between similar parts of OF-7-2 and OF-8-1-2-2. The orbit members shown in the plots have a z-amplitude $A_z \leq 0.05$ DU. The red to yellow portions represent orbits on OF-7-2. The green to blue portions represent orbits on the part of OF-8-1-2-2 in between the orbits corresponding to 8-1-2-2 and 8-1-3-1. The cyan to magenta portions represent orbits on OF-8-1-2-2 in between the orbits corresponding to 8-1-3-1 and 7-2-2-4. The gray portions represent orbits on OF-7-2 and OF-8-1-2-2 that have a z-amplitude $A_z > 0.05$ DU

Part B exists in simpler models. It should be noted that similar behavior was observed in the direct family, as can be seen in Fig. 3.

Another result that should be mentioned relates to the ridge line. As can be seen in the configuration space plots in several of the previous figures (e.g., Fig. 20), there appears to be many perpendicular crossings of the ridge line when looking at the orbits in the configuration space from the xy-view. This appears to indicate that viewing the state space in cylindrical coordinates (i.e., the hlz-frame used in Brown and Scheeres (2023a)) can provide more useful insight than just viewing the state space in the xyz-frame. This insight could be particularly useful when analyzing the eigenvectors of the monodromy matrix. This frame was also useful when analyzing the eigenvectors of the Jacobian matrix (Brown and Scheeres 2023b, a).

4.3.2 Persistence of underlying local structures

Parts of some families that lie in a more localized region of the space appear to be exhibit similar progressions. We will study the members of OF-7-2 and OF-8-1-2-2 as an example. The "vertical" members of these orbits were discussed previously in Sect. 4.3.1 (see Fig. 19), but we will now discuss the "planar" members of these families. The orbits on these two families with vertical amplitudes $A_z \leq 0.05$ DU were isolated and plotted in Fig. 22.

It appears the "planar" members progress in a nearly continuous manner. The discontinuities in this progression are encountered as the families head toward BPs corresponding to orbits with large vertical amplitudes, but these discontinuities are small when viewing the "planar" members from the xy-view. It is important to remember that OF-7-2 "absorbed" the first part of OF-7/8-3 after EP 8 transitioned from a stable center to an unstable center (see Fig. 8). This could help explain the near connection between OF-7-2 and OF-8-1-2-2. The connection between the green to blue portion and cyan to magenta portion of OF-8-1-2-2 appears to indicate the persistence of OF-7/8-3. Even though OF-7/8-3 could only be directly computed from a linearization about EP 8 for a limited range of slower spin rates when EP 8 was a stable center, this orbit structure (or at least an orbit structure very similar to it) appears to exist at the current spin rate, even though it cannot be directly accessed through a linearization about EP 8.

This behavior was seen in many of the other families identified in this work. While the similarities seen in Fig. 21 appear to be related to global symmetries, the similarities in Fig. 22

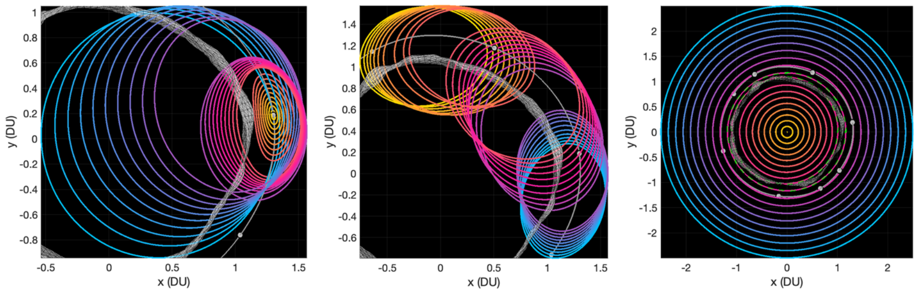

Fig. 23 Reconstructed TAEM families consisting of orbits computed using the polyhedron model. The reconstructed families are TAEM L1 (left), TAEM R0 (middle), TAEM L0 (right). Reconstructed TAEM L1: The members in the gold to orange portions are from OF-1-2, the members in the orange to purple portions are from OF-1-1, and the members in the purple to blue portions are from OF-2-1. Reconstructed TAEM R0: The members in the gold to orange portions are from OF-5/0-2, the members in the orange to purple portions are from OF-2-1, and the members in the purple to blue portions are from OF-1-1. Reconstructed TAEM L0: The members in the gold to magenta portions are from OF-5/0-2 and the members in the magenta to blue portions are from OF-2-1 (i.e., members from OF-1-0). The inner (outer) dashed green line represents the last (first) member of OF-5/0-2 (OF-2-1) family shown in this plot

appear to be related to local structures. It should be mentioned that this pattern of connections between parts of orbit families that have large changes in T but very small changes in C is similar in structure to the BFs connecting the long-period planar IF (e.g., OF-7/8-3, OF-3/4-3, etc.) to the other two IFs related to that particular EP pair when that center EP was stable.

4.3.3 Persistence of underlying global structures

The model of Bennu is similar to the shape of a triaxial ellipsoid if the right parameters are used. With that in mind, we would expect some of the orbits computed using the current polyhedron model to have similar characteristics to some of the orbits obtained by using a triaxial ellipsoid model. We will focus on three specific examples of the similarities, although there are many more. The perturbations present in this model seem to rip apart the underlying structure and piece it back together in different groupings. While the characteristics of the triaxial ellipsoid model used in Romanov and Doedel (2012) (which will be abbreviated as the TAEM for the remainder of this paper) are not based on Bennu, the overall progression of those families will be considered in this discussion. Orbits identified using the constant-density polyhedron model appear similar to the L1, R0, and L0 families identified in the TAEM. These TAEM families can be "reconstructed" using orbits from the constant-density polyhedron model, and the results are shown in Fig. 23.

For example, the L1 family in the TAEM (depicted in Figure 3(c) in Romanov and Doedel (2012)) can be viewed as starting at EP 1 and progressing continuously until the TAEM L0 family is reached. Along the way a BP corresponding to the TAEM A11 and TAEM A12 families and a BP corresponding to the TAEM R0 family are reached (Romanov and Doedel 2012). In the polyhedron model, OF-1-2 starts with a very similar progression (see Figs. 9 and 10). After a certain point, however, OF-1-2 appears to progress with members resembling those of the TAEM A11/A12 family. If we only collect the members of OF-1-2 before this point is reached, that group of orbits is very similar to part of the TAEM L1 family. We also see some orbits in OF-1-1 and OF-2-1 that are similar to the TAEM L1 family. By stitching together these three groups of orbits, we can construct a new group of orbits that is similar to the

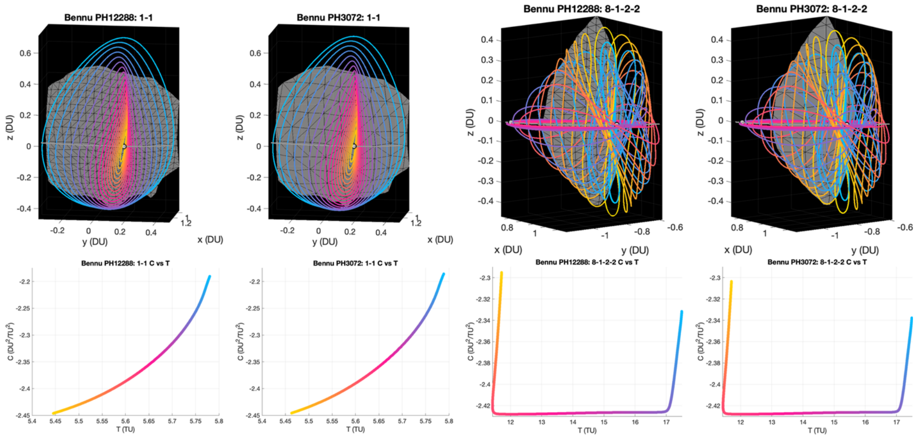

Fig. 24 Similarities between selected orbit families in the polyhedron model with 12,288 faces (PH12288) and the polyhedron model with 3,072 faces (PH3072). The first family is OF-1-1 which is shown from its first member up until the point where a member on the family crosses the surface for the first time. This family is depicted in the first and second columns of plots. The second family is OF-8-1-2-2 which is shown from its first member up until the member corresponding to 8-1-3-2. This family is depicted in the third and fourth columns of plots

TAEM L1 family. The discontinuities in this group of orbits are significant, but the overall progression of the members in this group appears to be similar.

Another example is the TAEM R0 family (depicted in Figure 4(d) in Romanov and Doedel 2012). Groups of orbits from OF-5/0-2, OF-2-1, and OF-1-1 were stitched together to obtain the reconstructed TAEM R0 family. The third and final example of these reconstructed families presented in this work is the TAEM L0 family (depicted in Figures 3(a) and 3(b) in Romanov and Doedel 2012). Groups of orbits from OF-5/0-2 and OF-2-1 were stitched together to obtain the reconstructed TAEM L0 family. It should be reiterated that the members of OF-2-1 are the same as members of OF-1-0. It is also important to note that the orbits from the polyhedron model used to reconstruct the TAEM families may not be the exact dynamical equivalent to the actual members of the TAEM families. However, for many structures in the TAEM, groups of orbits that were computed using the polyhedron model exhibit similar characteristics and progressions when stitched together as the original orbit structures in the TAEM.

We also computed all of the families presented in this work using a reduced polyhedron model of Bennu with only 3072 faces. The families identified using the current polyhedron model were virtually identical to the families identified using the reduced polyhedron model. This is additional evidence that, at least for nearly spherical asteroids like Bennu, many orbit structures identified in simplified models of the asteroid should be present when using more detailed models. OF-1-1 and OF-8-1-2-2 were selected to show the similarities between the families from the two models, and these families are shown in Fig. 24.

4.4 Preliminary discussion of mission applicability

While a large number of factors are considered when selecting orbits to use for spacecraft missions (such as specific scientific objectives, and communications requirements), we will narrow our analysis to focus on a limited set of orbits based on two characteristics. For the

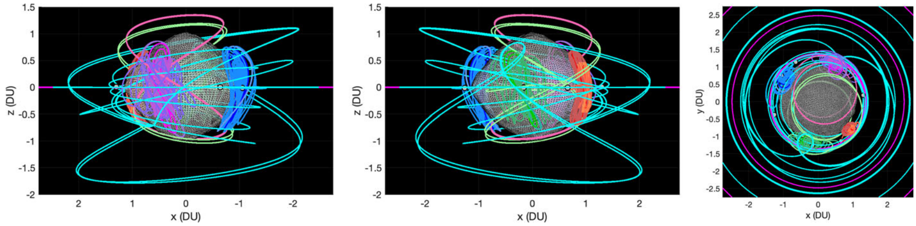

Fig. 25 Stable orbits that lie entirely outside the asteroid. The purple/pink lines are orbits that were computed near EP 2, the blue lines are orbits that were computed near EP 4, the green lines are orbits that were computed near EP 6, and the red/orange lines are orbits that were computed near EP 8. The magenta lines are orbits that are from OF-1-0 and the cyan lines are orbits that are from OF-2-0. Note the axes are cropped to focus on asteroids near the surface

majority of spacecraft missions, orbits that do not intersect the surface of the asteroid are required. Stable orbits are also desirable. For this reason our preliminary set of useful orbits, shown in Fig. 25, are those that are both stable and lie entirely outside the surface of the asteroid.

The cyan orbits in Fig. 25 that have significant vertical amplitudes are orbits that were obtained in the continuation scheme after previous members of the family had crossed the surface of the asteroid. These specific orbits were obtained because each family was continued beyond the point when a member crossed the surface. By continuing the families after an orbit crossed the surface, a more complete picture of the orbit family structure is obtained, as are more orbits with characteristics that are potentially useful for applications to spacecraft missions.

5 Conclusion

A large number of orbits in the vicinity of the asteroid Bennu were computed and analyzed using a constant-density polyhedron model based on measurements from the OSIRIS-REx mission. The planar retrograde and direct families, orbit families emanating from equilibria, and families emanating from bifurcation points in other families were identified and analyzed. Overall, there were many similarities to the structures identified using this model and the structures identified using simplified models like the homogeneous rotating gravitating triaxial ellipsoid. While the asteroid does not have any perfect symmetry, a number of the orbit structures identified were nearly symmetric. Furthermore, many of the structures identified in this analysis were very similar to each other, and we expect a number of these structures evolve in similar ways. Four distinct types of orbit families were identified emanating from bifurcation points on the set of initial families which emanated from equilibria. Continuing the computation of the orbit families beyond the point when a member intersected the surface of the asteroid yielded far more insight into how many of these structures fit together.

Acknowledgements This work was conducted with funding from the Solar System Exploration Research Virtual Institute and National Aeronautics and Space Administration Grant Number 80NSSC22K0240.

Author Contributions Not applicable.

Funding Not applicable.

Availability of data and materials The datasets generated during and/or analyzed during the current study are available from the corresponding author on reasonable request.

Declarations

Conflict of interest The authors declare they have no financial or non-financial interests that are directly or indirectly related to this work.

Ethics approval Not applicable.

Consent to participate Not applicable.

Consent for publication Not applicable.

Code availability Not applicable.

References

Barnouin, O., Daly, M., Palmer, E., et al.: Shape of (101955) Bennu indicative of a rubble pile with internal stiffness. Nat. Geosci. **12**(4), 247–252 (2019)

Benner, L.A.M., Busch, M.W., Giorgini, J.D., et al: Radar observations of near-earth and main-belt asteroids. In: Michel, P., DeMeo, F.E., Bottke, W.F. (eds) Asteroids IV. University of Arizona Press, pp. 165–182 (2015)

Broucke, R.A.: Stability of periodic orbits in the elliptic. Restricted three-body problem. AIAA J. **7**(6), 1003–1009 (1969)

Brown, G.M., Scheeres, D.J.: A global method to compute asteroid equilibrium points for any spin rate. In: 33rd AAS/AIAA Space Flight Mechanics Meeting (2023a)

Brown, G.M., Scheeres, D.J.: Studying the temporal evolution of the dynamical environment around asteroid (101955) Bennu. Icarus (2023b)

Bury, L.: Low-Energy Secondary-Body Landing Trajectories in the Three-Body Problem. PhD thesis, University of Colorado Boulder (2021)

Campbell, E.T.: Bifurcations from families of periodic solutions in the circular restricted problem with application to trajectory design. PhD thesis, Purdue University (1999)

Chappaz, L.P.: The dynamical environment in the vicinity of small irregularly-shaped bodies with application to asteroids. Master's thesis, Purdue University (2011)

Doedel, E.J., Romanov, V.A., Paffenroth, R.C., et al.: Elemental periodic orbits associated with the libration points in the circular restricted 3-body problem. Int. J. Bifurc. Chaos **17**(8) (2007)

Hénon, M.: Generating Families in the Restricted Three-Body Problem. Springer, Berlin (1997)

Hergenrother, C., Maleszewski, C., Nolan, M., et al.: The operational environment and rotational acceleration of asteroid (101955) Bennu from OSIRIS-REx observations. Nat. Commun. **10**(1291) (2019)

Hou, X., Xin, X., Feng, J.: Genealogy and stability of periodic orbit families around uniformly rotating asteroids. Commun. Nonlinear Sci. Numer. Simul. **56**, 93–114 (2018)

Howard, J.E., MacKay, R.S.: Linear stability of symplectic maps. J. Math. Phys. **28**(5) (1987)

Hu, W.D., Scheeres, D.J.: Periodic orbits in rotating second degree and order gravity fields. Chin. J. Astron. Astrophys. **8**(1), 108–118 (2008)

Jiang, Y., Baoyin, H.: Periodic orbit families in the gravitational field of irregular-shaped bodies. Astrono. J. **152**(5) (2016)

Jiang, Y., Baoyin, H.: Annihilation of relative equilibria in the gravitational field of irregular-shaped minor celestial bodies. Planet. Space Sci. **161**(15), 107–136 (2018)

Jiang, Y., Baoyin, H.: Periodic orbits related to the equilibrium points in the potential of Irregular-shaped minor celestial bodies. Results Phys. **12**, 368–374 (2019)

Jiang, Y., Li, H.: Equilibria and orbits in the dynamical environment of asteroid 22 Kalliope. Open Astronomy **28**(1), 154–164 (2019)

Jiang, Y., Baoyin, H., Li, J., et al.: Orbits and manifolds near the equilibrium points around a rotating asteroid. Astrophys. Space Sci. **349**(1), 83–106 (2014)

Jiang, Y., Baoyin, H., Li, H.: Periodic motion near the surface of asteroids. Astrophys. Space Sci. **360**(2) (2015a)

Jiang, Y., Yu, Y., Baoyin, H.: Topological classifications and bifurcations of periodic orbits in the potential field of highly irregular-shaped celestial bodies. Nonlinear Dyn. **81**(1–2), 119–140 (2015)

Kang, H., Jiang, Y., Li, H.: Convergence of a periodic orbit family close to asteroids during a continuation. Results Phys. **19** (2020)

Karydis, D., Voyatzis, G., Tsiganis, K.: A continuation approach for computing periodic orbits around irregular-shaped asteroids. An application to 433 Eros. Adv. Space Res. **68**(11), 4418–4433 (2021)

Lan, L., Yang, H., Baoyin, H., et al.: Retrograde near-circular periodic orbits near equatorial planes of small irregular bodies. Astrophys. Space Sci. **362**(9) (2017)

Lara, M., Scheeres, D.J.: Stability bounds for three-dimensional motion close to asteroids. J. Astronaut. Sci. **50**(4), 389–409 (2002)

Lauretta, D., DellaGiustina, D., Bennett, C., et al.: The unexpected surface of asteroid (101955) Bennu. Nature **568**, 55–60 (2019)

Li, X., Gao, A., Qiao, D.: Periodic orbits, manifolds and heteroclinic connections in the gravity field of a rotating homogeneous dumbbell-shaped body. Astrophys. Space Sci. **362**(4) (2017)

Liu, Y., Jiang, Y., Li, H.: Bifurcations of periodic orbits in the gravitational field of irregular bodies: applications to bennu and steins. Aerospace **9**(3) (2022)

Llanos, P., Miller, J., Hintz, G.: Orbital evolution and environmental analyses around asteroid 2008 EV5. In: Spaceflight mechanics meeting 2014 (2014)

MacMillan, W.D.: Theory of the Potential. Dover Publications Inc, New York (1958)

McMahon, J., Scheeres, D., Chesley, S., et al.: Dynamical evolution of simulated particles ejected from asteroid Bennu. J. Geophys. Res. Planets **158**(8), 1–18 (2020)

Ni, Y., Baoyin, H., Junfeng, L.: Orbit dynamics in the vicinity of asteroids with solar Perturbation. In: 65th International Astronautical Congress, pp. 4610–4620 (2014)

Ni, Y., Jiang, Y., Baoyin, H.: Multiple bifurcations in the periodic orbit around Eros. Astrophys. Space Sci. **361**(5) (2016)

Pedros-Faura, A., McMahon, J.W.: Effects of primary shadowing on asteroid ejecta captured into periodic orbits. In: 73rd International Astronautical Congress (2022)

Romanov, V.A., Doedel, E.J.: Periodic orbits associated with the libration points of the homogeneous rotating gravitating triaxial ellipsoid. Int. J. Bifurc. Chaos **22**(10) (2012)

Romanov, V.A., Doedel, E.J.: Periodic orbits associated with the libration points of the massive rotating straight segment. Int. J. Bifurc. Chaos **24**(4) (2014)

Scheeres, D.J.: Orbital Motion in Strongly Perturbed Environments. Springer, Berlin (2012)

Scheeres, D.J., Ostro, S.J., Hudson, R.S., et al.: Orbits close to asteroid 4769 castalia. Icarus **121**(1), 67–87 (1996)

Scheeres, D.J., Williams, B.G., Miller, J.K.: Evaluation of the dynamic environment of an asteroid: applications to 433 eros. J. Guid. Control. Dyn. **23**(3), 466–475 (2000)

Scheeres, D.J., Britt, D., Carry, B., et al.: Asteroid interiors and morphology. In: Michel, P., DeMeo, F.E., Bottke, W.F. (eds) Asteroids IV. University of Arizona Press, pp. 777–798 (2015)

Scheeres, D.J., Hesar, S.G., Tardivel, S., et al.: The geophysical environment of Bennu. Icarus **276**, 116–140 (2016)

Scheeres, D.J., French, A.S., Tricarico, P., et al.: Heterogeneous mass distribution of the rubble-pile asteroid (101955) Bennu. Sci. Adv. **6**(41):eabc3350 (2020)

Scheeres, D.J., Brown, G.M., Takahashi, S., et al.: The Dynamics about Asteroid (101955) Bennu. In: AIAA SCITECH 2022 Forum (2022)

Seydel, R.: Practical Bifurcation and Stability Analysis. Springer, Berlin (2010)

Tardivel, S.C.V.: The Deployment of Scientific Packages to Asteroid Surfaces. PhD thesis, University of Colorado Boulder (2014)

Werner, R.A., Scheeres, D.J.: Exterior gravitation of a polyhedron derived and compared with harmonic and mascon gravitation representations of asteroid 4769 Castalia. Celest. Mech. Dyn. Astron. **65**(3), 313–344 (1996)

Yu, Y., Baoyin, H.: Generating families of 3D periodic orbits about asteroids. Mon. Not. R. Astron. Soc. **427**(1), 872–881 (2012)

Yu, Y., Baoyin, H.: Orbital dynamics in the vicinity of asteroid 216 Kleopatra. Astrono. J. **143**(3) (2012b)

Yu, Y., Baoyin, H., Jiang, Y.: Constructing the natural families of periodic orbits near irregular bodies. Mon. Not. R. Astron. Soc. **453**(3), 3269–3277 (2015)

Zimovan-Spreen, E.M., Howell, K.C., Davis, D.C.: Near rectilinear halo orbits and nearby higher-period dynamical structures: orbital stability and resonance properties. Celestial Mech. Dyn. Astron. **132**(5) (2020)